

# Fingerprint Matching with Localized Deep Representation

Yongjie Duan\*, Zhiyu Pan\*, Jianjiang Feng, *Member, IEEE*, Jie Zhou, *Senior Member, IEEE*

**Abstract**—Compared to minutia-based fingerprint representations, fixed-length representations are attractive due to simple and efficient matching. However, fixed-length fingerprint representations are limited in accuracy when matching fingerprints with different visible areas, which can occur due to different finger poses or acquisition methods. To address this issue, we propose a localized deep representation of fingerprint, named LDRF. By focusing on the discriminative characteristics within local regions, LDRF provides a more robust and accurate fixed-length representation for fingerprints with variable visible areas. LDRF can be adapted to retain information within any valid area, making it highly flexible. The matching scores produced by LDRF also exhibit intuitive statistical characteristics, which led us to propose a matching score normalization technique to mitigate the uncertainty in the cases of very small overlapping area. With this new technique, we can maintain a high level of accuracy and reliability in our fingerprint matching, even as the size of the database grows rapidly. Our experimental results on 21 datasets containing over 140K fingerprints of various finger poses and impression types show that LDRF outperforms other fixed-length representations and is robust to sensing technologies and impression types. Besides, the proposed matching score normalization effectively reduces the false match rate (FMR) in large-scale identification experiments comprising over 5.11 million fingerprints. Specifically, this technique results in a reduction of two orders of magnitude compared to matching without matching score normalization and five orders of magnitude compared to prior works.

**Index Terms**—Fingerprint Matching, Fixed-Length Representation, Hamming Distance, Binomial Distribution, Deep Learning.

## I. INTRODUCTION

FINGERPRINT has been a popular biometric in various applications, including access control, national ID card, and law enforcement [1]. A fingerprint recognition system consists of three main modules: image acquisition, feature extraction, and matching. The feature extraction algorithm aims to extract discriminative features from fingerprints captured by fingerprint sensors. And the matching algorithm takes the extracted features of two fingerprints as inputs to calculate matching score. Typically, a fingerprint is represented as a collection of minutiae, which is demonstrated to present many advantages for fingerprint matching, including (1) the definition of minutia is clear and consistent with features utilized by human experts, thus ensuring compatibility across different

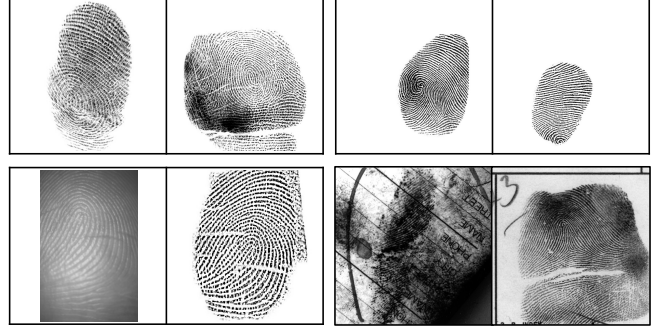


Fig. 1. Due to significant intra-class variations caused by different finger poses, sensing techniques, and impression types, it is very challenging to extract distinctive, consistent, and compact fixed-length representations of fingerprints.

algorithms [2]; (2) the distribution of minutiae location is highly random and contains sufficient discriminative information for identification [3]; (3) automatic minutiae extraction is robust to noise thanks to contextual filtering [4], [5], (4) good recognition performance can be achieved even by traditional point matching algorithms [6], [7]; (5) the template size is small and thus adopted as the standard template in many applications [8]. Thanks to the aforementioned benefits of minutia-based fingerprint representation, fingerprint recognition technique was able to find real applications in the early stages of artificial intelligence (around the 1970s) [9]. Up to date, most fingerprint matchers still utilize minutiae, with the exception of matchers in some smartphones, which use tiny fingerprint sensors [10].

However, minutia-based fingerprint representation poses several challenges: (1) High computational complexity. Combining slow minutiae matching with efficient candidate filtering approaches is usually required for large-scale fingerprint identification systems [11], [12], making the entire system very complex and possibly reducing the recognition accuracy; (2) Drastic performance degradation in fingerprints of low quality. Additional fingerprint features are introduced to improve the matching performance [13], [14], while further increasing the computation and storage cost; (3) Difficult template encryption. Currently available template encryption technologies for minutia sets are far fewer than those for fixed-length representations [15], and tend to result in significant performance reduction [16]; (4) Hard to model the statistical distributions of distance between genuine or impostor pairs [17]–[19]. This makes it difficult to obtain reliable and accurate random match probability prediction like DNA typing

\* Corresponding authors contributed equally to this work.

Y. Duan, Z. Pan, J. Feng, and J. Zhou are with Department of Automation, Beijing National Research Center for Information Science and Technology, Tsinghua University, Beijing 100084, China (e-mail: dyj17@mails.tsinghua.edu.cn; pzy20@mails.tsinghua.edu.cn; jfeng@tsinghua.edu.cn; jzhou@tsinghua.edu.cn).

[20], which is very important for forensic applications [21]; (5) Difficult to implement minutiae matcher as end-to-end deep networks. Although several intermediate steps can be implemented by deep networks, such as extracting minutiae [22], [23] and their local descriptors [24], it is hard to optimize the whole fingerprint matcher if not implemented as end-to-end deep networks.

Therefore, researchers have proposed several fixed-length fingerprint representations, with the aim for fingerprint indexing [24]–[31], template security [27], [32]–[34], and matching low quality fingerprints [35], [36]. Conventional fixed-length fingerprint representations are usually defined by local responses of multiple Gabor filters [35], parameters of orientation field model [37], [38], local minutiae vicinities [39], histograms of minutia triplets or pairs features [33], [40], local ridge orientation and frequency [25], and local discretized texture descriptors [34]. The accuracies of these representations are typically much lower than those achieved by state-of-the-art (SOTA) minutiae matchers. With the rapid development of deep learning technology, more recently, fixed-length representations were extracted utilizing deep networks from aligned fingerprints [24], [27], [31]. Such methods present excellent performance on fingerprints with complete area such as rolled fingerprints. However, background area is not negligible and may dominate in fingerprints with diverse visible areas and impression types, particularly when fingerprint areas are small, resulting in a dramatic decrease in the matching performance. Although minutia information was introduced in several approaches explicitly [28], [30] and implicitly [29], the accuracy of minutia extraction itself may be compromised. Additionally, the matching is also not restricted within the overlapping area since the global aggregation step in such methods erases both the number and location information of minutiae, which limits the applicability of such methods for matching fingerprints with diverse visible areas. Extracting pyramid features at different scales and concatenating them as a feature vector was considered in [36]. However, matching performance is still affected by the coarse local region division and fusing weights for different fingerprints in such methods. Besides, extraction these multi-scale features also consumes higher computational resources and storage space.

Up to date, fixed-length fingerprint representations have primarily demonstrated good performance on rolled fingerprints and are mainly beneficial for expediting large-scale identification systems utilizing rolled fingerprints. However, it still cannot be considered as a universal fingerprint representation like minutia set. A universal representation of fingerprints needs to present satisfactory performance not just on rolled fingerprints but also on more common fingerprints with incomplete area and diverse finger poses (e.g., plain or latent fingerprints).

Therefore, in this paper, we propose a localized deep representation of fingerprint, named LDRF, to achieve efficient and accurate fingerprint matching, particularly for images with diverse visible areas and impression types. The first step in our proposed method is to align the fingerprint using a fingerprint pose estimation approach [41]. Next, we extract the localized representation of the fingerprint and identify the valid area.

To incorporate global constraints, we utilize a 2D positional embedding technique that introduces global position information into the fixed-length representations. This module enables the network to pay more attention to distinct characteristics that present across different local regions, and thus helps to improve performance. Furthermore, considering only feature embeddings in overlapping area, any irrelevant or invalid data that may interfere with the matching process can be eliminated from the extracted representations. Consequently, our method can achieve good performance even after simple representation binarization. This is particularly useful for efficient searching of large-scale databases and for template encryption.

Besides, the proposed localized deep representation exhibits intuitive and theoretically consistent statistical characteristics. Specifically, the distribution of the distance between impostor pairs conforms well to the theoretical Binomial (for binary vectors) and Beta (for real-value vectors) distributions. Inspired by Daugman et al. [42], [43], we proposed a matching score normalization method that can effectively unify the reliability of matching scores for fingerprint pairs with different overlapping areas. Additionally, statistical modeling of the impostor matching score distribution enables us to reliably estimate matching performance for even larger population. This capability is crucial in forensic applications [21], where the accuracy and reliability of evidence can have a significant impact on the outcome of a case.

To verify the generalization ability of the proposed representation, it is necessary to evaluate it on datasets containing various fingerprint types. Therefore, evaluation was performed on 21 different datasets containing over 140K fingerprints with varying visible areas and impression types, including rolled, plain, latent, and contactless fingerprints, which is more comprehensive than previous fixed-length representation studies. And several datasets utilized are quite challenging for fixed-length representations, e.g., fingerprints with diverse finger poses and small image size. The experimental results obtained from these datasets consistently demonstrate the superiority of LDRF compared to other fixed-length representations. A large-scale database containing over 5.11 million fingerprints was also utilized to demonstrate the effectiveness of the proposed matching score normalization technique in improving identification performance for large population.

The remainder of the paper is organized as follows: Section II provides a review of prior works related to fixed-length representation. In Section III, we described the proposed localized deep representation. We introduce a matching score normalization method based on the statistical analysis of fingerprint matching scores in Section IV. Experimental results and limitations are presented in Sections V and VI, respectively. Lastly, in Section VII, we summarize our work.

## II. RELATED WORKS

Fixed-length fingerprint representations can be classified into two categories: alignment-based and alignment-free.

Fingerprint alignment is first performed in alignment-based approaches, and then fixed-length fingerprint representations are extracted from the aligned fingerprints. Intuitively, the accuracy of fingerprint alignment is crucial for the performance

of extracted features in such methods. Jain et al. [35] utilized multiple Gabor filters with different orientations to extract texture information, then the fixed-length representation was obtained by calculating standard deviation in a number of sectors defined with respect to the reference point, named FingerCode. Traditional fingerprint features, e.g., local ridge orientation, consistency, frequency, and minutia vicinities, can also be composed as fixed-length representations [25], [39]. But much lower performance is obtained using such representations compared to the SOTA minutia-based matcher due to the inaccurate and inconsistent feature extraction, which is mainly caused by low ridge quality and strong distortion. With the rapid development of deep learning, several researchers attempted to utilize deep networks to extract more discriminative features. Cao et al. [24] first proposed to extract deep features from aligned fingerprints. Engelsma et al. [27] then integrated fingerprint alignment and feature extraction into a single end-to-end network. Grosz et al. [31] combined the complimentary representations of attention-based and CNN-based embedding to further improve the fingerprint recognition ability. Good performance is obtained using such methods on fingerprints with large and complete fingerprint area such as rolled fingerprints. While for fingerprints with incomplete areas, background information is incorporated and even dominates in the extracted global features, which inevitably affects the matching performance. Song and Feng [26] then proposed to integrate pyramid features extracted from different local regions into a global fixed-length representation, although, incomplete fingerprint area was still not considered. Gu et al. [36] extracted pyramid features from various local regions, and the matching process was adopted within each local region to alleviate the issue of incomplete areas. However, the division of local regions is coarse and may lead to disregarding matching results in regions with small overlap, thereby inevitably decreasing the overall matching performance. Besides, the weights associated with fusing local regions need to be optimized across diverse datasets, affecting its generalization ability. Such methods also require a higher consumption of both memory and computational resources.

For alignment-free approaches, minutia information was usually incorporated. Song et al. [28] extracted local features around each minutia and aggregated them to a global fixed-length representation via an aggregation network. Wu et al. [30] followed the similar schematic and applied multi-task learning to provide auxiliary constraints for extracting local features around minutiae. Li et al. [29] introduced minutia information implicitly by a fully convolutional network and aggregated local descriptors via global average pooling. Grosz et al. [44] utilized vision transformer (ViT) [45] to integrate minutia map and original fingerprint. Such methods introduce minutia information, although, minutia extraction itself can be affected by various factors. Besides, the number and location of minutiae are lost after aggregation, resulting in a decreased discriminative ability of the extracted features.

The representation proposed in this paper is alignment-based, and to alleviate the impacts of inaccurate fingerprint alignment, a fingerprint pose estimation algorithm, which achieves the SOTA performance on various fingerprint types

[41], was utilized before extracting representations.

### III. LOCALIZED DEEP REPRESENTATION

We proposed to extract localized deep representations from fingerprints with different visible areas and impression types, including rolled, plain, latent, and contactless fingerprints. Different from minutia-based matching, fingerprints were first aligned by the estimated fingerprint poses [41], then the localized representations were extracted and valid area, i.e., fingerprint mask, was determined simultaneously. Matching score can be then calculated by removing information outside the overlapping area from the extracted representations. Benefiting from the intuitive and theoretically consistent statistical characteristics of matching scores using LDRF, we further proposed a matching score normalization method, which is discussed in Section IV. The overall schematic illustration of fingerprint matching using LDRF is shown in Fig. 2.

#### A. Representation Extraction

Considering the potential missing or noisy region of fingerprints in real applications, instead of extracting global deep representations investigated in prior works [24], [27], we extract a localized deep representation of fingerprint, named LDRF. Details of the proposed network architecture is shown in Fig. 3. The proposed network consists of three main modules: fingerprint alignment, localized feature extraction, and auxiliary minutia extraction. Note that the minutia extraction is designed as an auxiliary task for network training and is removed during inference to reduce computational cost.

1) *Fingerprint Alignment*: Fingerprint alignment has been demonstrated to be crucial and effective in various fingerprint recognition tasks, e.g., orientation field estimation [46]–[48], distortion detection and rectification [49]–[52], singularities detection [53], and fingerprint matching [24], [27], [35], [36]. Good alignment is conducive to both matching accuracy and efficiency. Training a network to extract robust and discriminative features can also be made less difficult after fingerprint alignment by reducing the variations of fingerprint poses. Therefore, for a better extraction of fixed-length representation, it is imperative to have a precise alignment of fingerprints. This study utilizes a dense voting algorithm [41] to determine fingerprint pose, which delivers SOTA performance for various fingerprint types. Pose estimation can get the center and vertical direction of a specific fingerprint. Then the fingerprint image is rotated to make the fingerprint coordinate align with the image coordinate. The center point is at the center of the image and the direction is vertical in the aligned image. After alignment, all fingerprints are in the same image coordinate, and the image resolutions of these aligned fingerprints are also as same as the original fingerprint resolution. Considering the compromise between computational efficiency and performance, we cropped the aligned fingerprint to  $512 \times 512$  and subsequently scaled it down to  $256 \times 256$  as input for the succeeding modules.

2) *Localized Feature Extraction*: ResNet-34 [54] was utilized as the network backbone to extract discriminative features. To retain more details of ridges, we removed the first

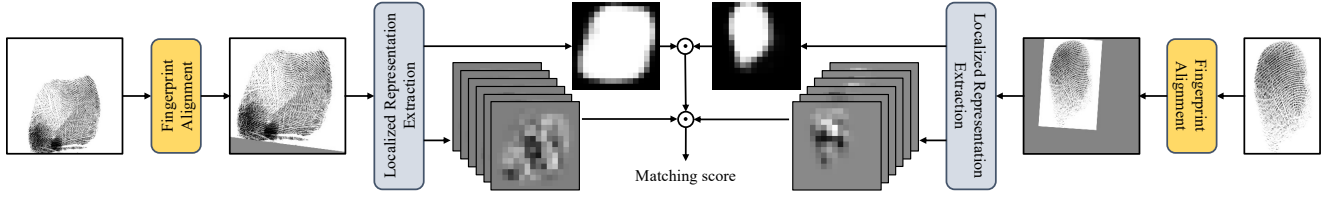


Fig. 2. Overview of fingerprint matching using the proposed LDRF.

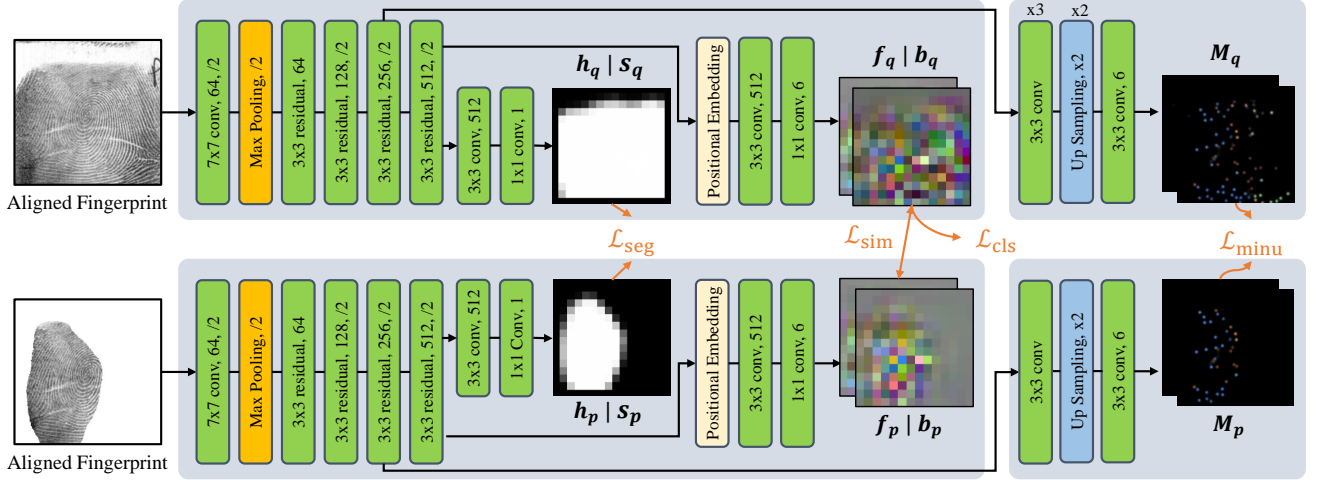


Fig. 3. Network architecture of LDRF and supervision losses used for training. We denote “conv” as 2D convolution layer, and “residual” as residual block. “|” is used to separate continuous representation or binary representation.

max pooling layer, resulting in an output size that is  $1/16$  of the input size, specifically  $16 \times 16$  in this study.

Different from global representations, local information was focused using such feature extraction strategy. In this study, to incorporate global constraints, we employed a 2D positional embedding module [55], [56]. The introduced global positional information enables the network to focus on distinct characteristics across different local regions, resulting in a more refined and detailed feature representation. Denote the channel number of the feature map as  $d_{\text{model}}$ , then the 2D positional embedding

$$\begin{aligned}
 PE(x, y, i) &= \sin(t(x, i)), \\
 PE(x, y, i + d_{\text{model}}/4) &= \cos(t(x, i)), \\
 PE(x, y, i + 2 * d_{\text{model}}/4) &= \sin(t(y, i)), \\
 PE(x, y, i + 3 * d_{\text{model}}/4) &= \cos(t(y, i)),
 \end{aligned} \tag{1}$$

where  $(x, y)$  refers to the two-dimensional coordinate indices of the feature map,  $i$  is the index for channel dimension and  $i \in [0, d_{\text{model}}/4)$ ,

and the function  $t(x, i)$  or  $t(y, i)$  is computed by

$$t(\text{pos}, i) = \frac{\text{pos}}{10000^{4i/d_{\text{model}}}}, \tag{2}$$

was added to the output of the backbone, and followed by two convolution layers to obtain the localized fingerprint features ( $d \times 16 \times 16$ ,  $d = 6$  in this study).

Apart from the localized features, a valid area was also estimated to determine regions conveying essential and reliable

ridge information. The estimated valid area has the same 2D resolution, which is  $16 \times 16$ , as the features extracted from fingerprints. Given the valid area, the localized features can be adapted by Hadamard production to eliminate extraneous information. Only feature embeddings within the overlapping area are utilized for representation comparison.

3) *Auxiliary Minutia Extraction*: The location and orientation of minutiae contain sufficient information for identity recognition, as demonstrated in various minutia-based matching methods [3], [57]–[61]. Therefore, we also attempted to introduce minutia information in the extracted representations via multi-task learning.

As the number and location of minutiae vary across different impressions, we converted all minutiae of a fingerprint to a 6-channel heatmap using different ranges of orientations inspired by the minutia domain knowledge [27]. The ground truth of the minutia heatmap was generated by summarizing the contributions of minutiae locations within each range of orientation. Fig. 4 shows an example of a minutia heatmap by regrouping the six channels minutia map into two RGB color maps for better visualization.

Considering that minutia was classified as a type of local feature, i.e., level-2 feature [53], the output of the penultimate residual module of the backbone was utilized as the input for minutia extraction. The minutia extraction module consists of two up-sampling and convolution layers, which means the size of the estimated minutia heatmap is  $128 \times 128$ . Additionally, skip connection was employed to integrate coarse and fine information during up-sampling [62]. Since all elements in

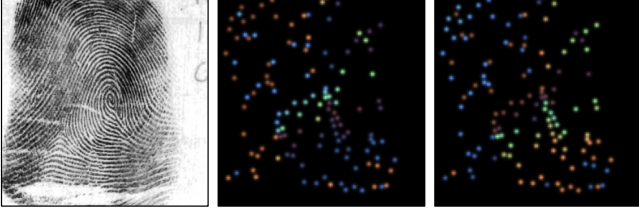


Fig. 4. An example of minutia map. The minutia locations and orientations are represented by a 6-channel heatmap, which is shown by two 3-channel RGB color maps for better visualization.

minutia heatmap are non-negative, a ReLU activation layer was added after the final layer of minutia extraction module to normalize the output values.

### B. Fingerprint Matching

Given a pair of fingerprints  $(p, g)$ , the extracted localized deep representations are denoted as  $f_q \in \mathbb{R}^{d \times 16 \times 16}$  and  $f_g \in \mathbb{R}^{d \times 16 \times 16}$ , and also the estimated valid area as  $h_q \in \mathbb{R}^{1 \times 16 \times 16}$  and  $h_g \in \mathbb{R}^{1 \times 16 \times 16}$ . Dimension broadcasting was first adopted to unify the dimensions and followed by a vector flattening, i.e.,  $f_q \in \mathbb{R}^{256d}$ ,  $f_g \in \mathbb{R}^{256d}$ ,  $h_q \in \mathbb{R}^{256d}$ , and  $h_g \in \mathbb{R}^{256d}$ .

The matching score is obtained by calculating the cosine similarity between the flattened features. Only the feature embeddings within the overlapping area are considered during comparison. Specifically, the matching score of fingerprint pair  $(p, g)$  is computed by

$$s(q, g) = \frac{1}{2} \cdot \frac{\langle f'_q, f'_g \rangle}{\|f'_q\| \|f'_g\|} + \frac{1}{2}, \quad (3)$$

where  $f'_q$  and  $f'_g$  are the transformed localized representations

$$f'_q = f_q \odot h_{q \cap g}, \quad f'_g = f_g \odot h_{q \cap g}. \quad (4)$$

$\odot$  denotes the dot product, and  $h_{q \cap g}$  is the overlapping area

$$h_{q \cap g} = h_q \odot h_g. \quad (5)$$

### C. Binary Representation

Quantization is widely used in biometric recognition to reduce the consumption of storage and computational resources [60], [63]. In this study, we also attempted to binarize the representations while not decreasing the performance drastically.

Fig. 5b shows the distribution of representation elements extracted by our method, which presents good symmetry centered on zero. Thus, we implemented a simple binarization method: elements larger than 0 are assigned Boolean “true”, and “false” otherwise. Fig. 5a and Fig. 5c show an example of the extracted 6-channel localized representation and its binarization respectively. The predicted valid area  $h$  is also binarized using different thresholds of extracting ridges in fingerprints with different visible areas and ridge qualities, i.e., 0.1 for rolled or plain fingerprints, and 0.5 for latent fingerprints, to get  $s$ . Finally, the size of the binarized representation is reduced to 224 bytes (1536 + 256 = 1792 bits).

Given two binarized representations, although similarity can be calculated using Eq. (3), a more rational and intuitive measure of dissimilarity is Hamming distance

$$\text{HD}(q, g) = \frac{\|(b_q \oplus b_g) \cap s_q \cap s_g\|}{\|s_q \cap s_g\|}, \quad (6)$$

where  $\oplus$  denotes xor operation,  $b$  and  $s$  are the binarized vectors of  $f$  and  $h$  respectively. Then the matching score of fingerprint pair  $(p, g)$  can be obtained by

$$s(q, g) = 1 - \text{HD}(q, g). \quad (7)$$

### D. Objective Functions

The proposed network aims to extract robust and discriminative representations, and the following provides detailed descriptions of the objective functions used in this study.

1) *Classification Loss*: Inspired by face representation learning [64]–[66], fingerprint representation extraction can also be optimized by classifying the extracted features as corresponding fingers. However, unlike face recognition, the number of impressions per finger is much fewer in most fingerprint databases. Therefore, CosFace [66], which has been proven to be effective to enlarge classification margins between different categories, was utilized for optimization in this study. Specifically, the extracted fingerprint feature was first flattened and followed by a FC layer with  $C$  classes. The CosFace loss function is modified based on SoftMax

$$\mathcal{L}_{\text{cls}} = -\frac{1}{N} \sum_{n=1}^N \log \frac{e^{A(\cos(\theta_{y_n}) - b)}}{e^{A(\cos(\theta_{y_n}) - b)} + \sum_{c=1, c \neq y_n}^C e^{A \cos(\theta_c)}}, \quad (8)$$

where  $\cos(\theta_c)$  is calculated by

$$\cos(\theta_c) = W_c^T f_n, \quad W_c = \frac{W_c}{\|W_c\|} \quad f_n = \frac{f_n}{\|f_n\|}. \quad (9)$$

The hyper-parameter  $A$  is utilized for magnitude normalization,  $b$  denotes the margin,  $N$  is the number of samples within a batch, and  $y_n$  is the class label of sample  $f_n$ . By introducing the parameter  $b$ , the division margin between different classes is enlarged while compressing the intra-distance within the same category, thus improving the classification performance.

2) *Segmentation Loss*: For valid area prediction, the binary cross-entropy loss function was utilized for optimization

$$\mathcal{L}_{\text{seg}} = -\frac{1}{|\Omega|} \sum_{(i,j) \in \Omega} (g^{ij} \log(h^{ij}) + (1 - g^{ij}) \log(1 - h^{ij})), \quad (10)$$

where  $(i, j) \in \Omega$  indicates coordinates across the output map,  $h$  represents the predicted probability map of the valid area, and  $g$  denotes the ground truth.

3) *Minutia Extraction Loss*: For minutia heatmap prediction, we adopted mean square error loss for supervision

$$\mathcal{L}_{\text{minu}} = \frac{1}{|\Omega|} \sum_{(i,j,k) \in \Omega} \|M(i, j, k) - M^*(i, j, k)\|^2, \quad (11)$$

where  $M$  is the estimated heatmap and  $M^*$  is the ground truth.

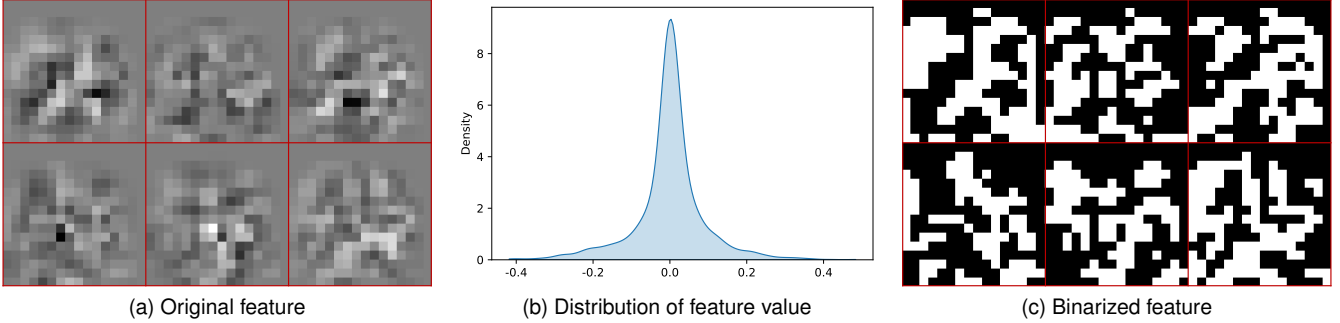


Fig. 5. An example of template binarization.

4) *Local Similarity Loss*: Given that  $\mathcal{L}_{\text{cls}}$  considers all elements of the extracted localized representations, the features from incomplete fingerprints cannot be directly optimized. Consequently, we proposed a “teaching-mimicking” tactic, wherein features extracted from incomplete fingerprints mimic those found in complete fingerprints to uphold consistency in representations across fingerprints of various visible areas, intensity distributions, and distortion patterns originating from the same finger. Specifically, the loss function is defined by

$$\mathcal{L}_{\text{sim}} = \frac{1}{|h_q \cap g|} \sum_{(i,j) \in h_q \cap g} \|f_q^{ij} - f_g^{ij}\|^2, \quad (12)$$

where  $f_q$  and  $f_g$  denote the representations extracted from incomplete and complete fingerprints respectively.

Note that only the features extracted from rolled fingerprints were supervised by  $\mathcal{L}_{\text{cls}}$ , and the features from incomplete fingerprints were considered in  $\mathcal{L}_{\text{sim}}$ .

5) *Overall Loss*: Consequently, the proposed network was supervised by optimizing the overall objective function

$$\mathcal{L} = \mathcal{L}_{\text{cls}} + \lambda_{\text{seg}} \mathcal{L}_{\text{seg}} + \lambda_{\text{minu}} \mathcal{L}_{\text{minu}} + \lambda_{\text{sim}} \mathcal{L}_{\text{sim}}, \quad (13)$$

where  $\lambda_{\text{seg}}$ ,  $\lambda_{\text{minu}}$ , and  $\lambda_{\text{sim}}$  are trade-off parameters for  $L_{\text{seg}}$ ,  $L_{\text{minu}}$ , and  $L_{\text{sim}}$  respectively. In this paper, we set  $\lambda_{\text{seg}} = 1$ ,  $\lambda_{\text{minu}} = 0.01$ , and  $\lambda_{\text{sim}} = 0.00125$  to achieve roughly the same decreasing rate for those loss functions.

### E. Implementation Details

Due to limitations on the number of impressions from the same finger or the number of finger identities available in public fingerprint databases, a complex data augmentation was applied in this study to simulate multiple impressions from the same finger, thus increasing the diversity of training data to avoid over-fitting. Specifically, we utilized the distortion model obtained by Si et al. [49] and randomly generated different distortion fields, which were then applied on real fingerprints to simulate impressions with different distortion patterns. Histogram matching of intensity was then employed to adjust the intensity distribution of synthetic fingerprints with arbitrary plausible distributions in FVC2004 DB1A dataset, which aims to increase the variations of intensity distribution in synthetic fingerprints.

The proposed method was implemented using PyTorch on NVIDIA GeForce 3090 and trained from scratch. In addition

to the above training fingerprints simulation, additional data augmentation was also adopted, including random translation in range of 10 pixels and random rotation to follow a uniform distribution  $[-5^\circ, 5^\circ]$ . The normalization parameter  $A$  and margin  $b$  in Eq. (8) are set to 30 and 0.4, respectively. AdamW optimizer with initial learning rate of 0.00035 was utilized for network training. Learning rate decays by 0.1 after 10 epochs without performance improvement on validation dataset. And early stopping was performed after three times learning rate decays. Furthermore, L2 regularization on trainable parameters was also utilized to avoid over-fitting.

## IV. STATISTICAL ANALYSIS ON FINGERPRINT MATCHING

We conducted a statistical analysis of matching scores between fingerprint pairs using LDRF and then proposed a matching score normalization method based on the statistical modeling.

### A. Statistical Modeling for Fingerprint Matching

The binarized representations, described in Section III-C, were first used to facilitate intuitive analysis and comprehension. Then the statistical analysis was extended to the original representations in real values.

Given two binary vectors, their distance can be calculated by the number of different bits (see Eq. (6)). Then 1-to-1 fingerprint matching (whether two fingerprints arise from the same finger) can be modeled as a test of statistical independence. Specifically, when comparing two bits, only two possible results can be obtained: either they are the “same” or “different”. The vector length  $n$  indicates the number of such bit comparisons. Fig. 6 shows examples of binary difference of genuine pair and impostor pair.

Intuitively, this test of statistical independence is equivalent to toss a coin  $n$  times, with “heads” indicating two bits are different for example. Then the fairness of the coin can be determined by counting the proportion of “heads”: two vectors are independent (two fingerprints arisen from different fingers) when the proportion is roughly 50-to-50; whereas a strong evidence that two fingerprints come from the same finger if there is a preponderance of bits agreement. Obviously, impostor matching presents a good correspondence with tossing a fair coin randomly.

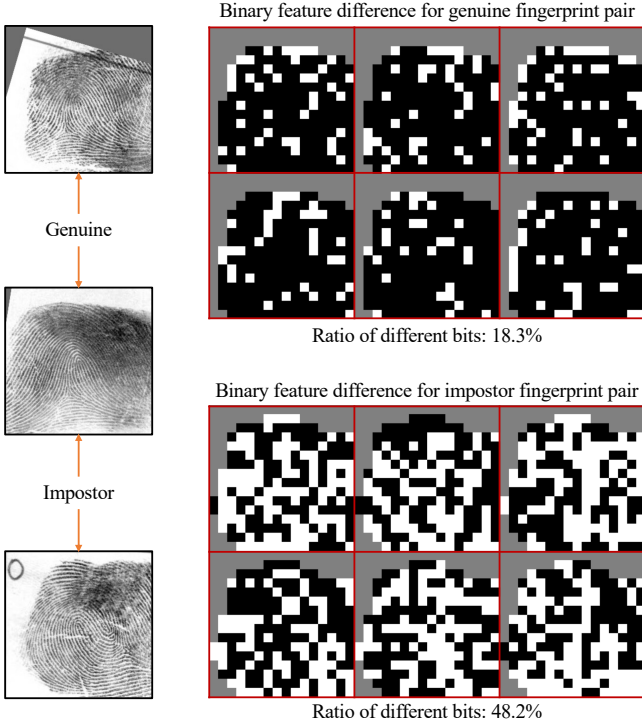


Fig. 6. Examples of differences between binary representations of genuine pair and impostor pair. White pixels indicate different bits.

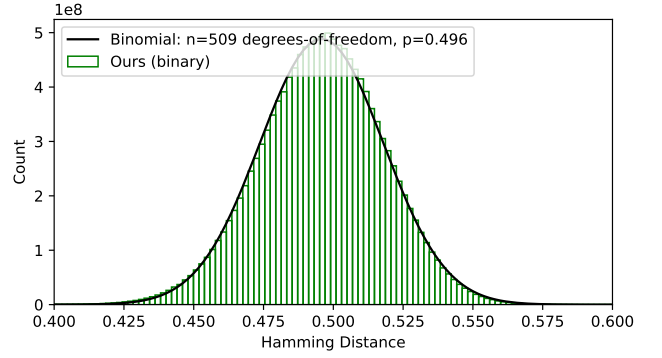
A single coin toss is known as a Bernoulli trial, whose result follows a Bernoulli distribution with parameter  $p$  indicating the probability of “heads”. And the result of  $n$  Bernoulli trials follows a Binomial distribution. Denote  $x$  as the number of “heads” in  $n$  Bernoulli trials, then the random variable  $x' = x/n$  also follows a Binomial distribution with probability mass function as:

$$P(x') = P\left(\frac{x}{n}\right) = C_n^x p^x (1-p)^{n-x} = \frac{n!}{x!(n-x)!} p^x (1-p)^{n-x}. \quad (14)$$

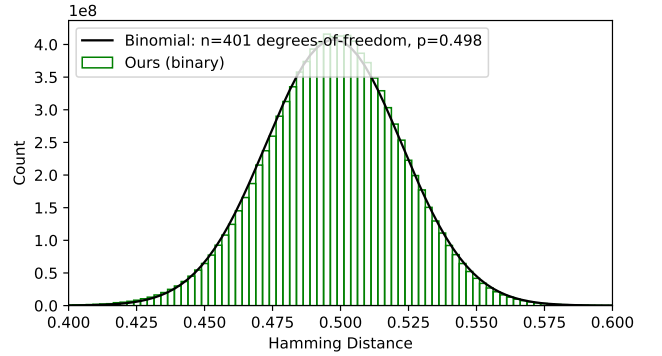
The expectation and variance of  $x'$  can be deduced as  $p$  and  $p(1-p)/n$ , respectively. We found that  $x'$  has the same meaning as Hamming distance in Eq. (6), i.e.,  $x$  pairs of bits are different between two vectors of length  $n$ . Consequently, the distribution of distance between impostor pairs using binary representations can be modeled as a Binomial distribution with expectation of  $p$  and variance of  $p(1-p)/n$ .

In order to evaluate the confidence and reliability of the aforementioned statistical analysis, a large dataset consisting of more than 5.11 million rolled fingerprints (5,114,826 fingerprints from different fingers<sup>1</sup>) was utilized. Specifically, we selected the last 2,700 pairs rolled fingerprints of NIST SD14 and extended the gallery using this large dataset (denoted as NIST SD14 extended dataset). We also extended N2N Plain (denoted as N2N Plain extended dataset) which presents more variations in area between fingerprints.

<sup>1</sup>This dataset is not utilized in the following algorithm training and testing since there is only one impression per finger



(a) NIST SD14 extended dataset



(b) N2N Plain extended dataset

Fig. 7. Distributions of Hamming distance of impostor pairs on extended datasets and the corresponding theoretical Binomial distributions whose parameters are determined by the observed distributions.

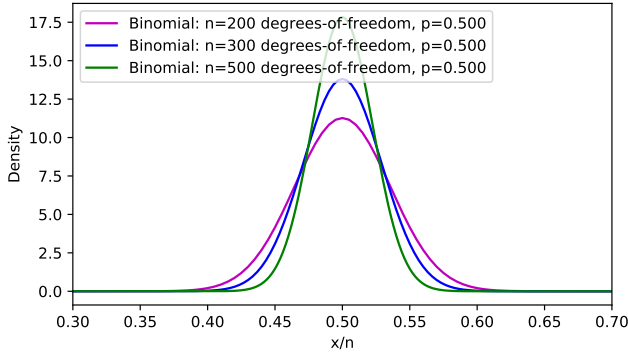
According to the experimental settings, NIST SD14 extended dataset has 2,700 genuine pairs and more than 13.8 billion impostor pairs ( $2700 \times 5117525 = 13817317500 \approx 1.38 \times 10^{10}$ ). For N2N Plain extended dataset, the number of genuine pairs is 2,000 and impostor pairs more than 10.2 billion ( $2000 \times 5116825 = 10233650000 \approx 1.02 \times 10^{10}$ ).

Fig. 7 shows the distributions of Hamming distance between impostor pairs on two extended datasets. Theoretical Binomial distributions, whose parameters  $n$  and  $p$  are calculated from the observed distributions of impostor pairs, are also drawn in black. It can be observed that the observed data fits well to the theoretical Binomial distribution, which demonstrates the validity of modeling the distance distribution between impostor pairs as a Binomial distribution.

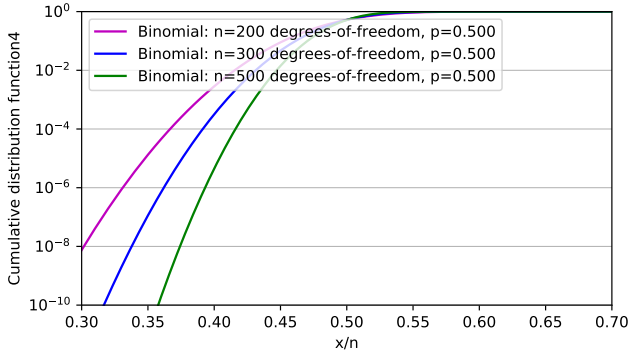
Then back to the original representations in real values, the cosine similarity between two independent random Gaussian vectors has been proven to follow a Beta distribution [67], which means the distribution of impostor scores using representations in real values can be modeled as a Beta distribution  $\text{Beta}(\frac{n-1}{2}, \frac{n-1}{2})$  with probability density function as:

$$P(s) = \frac{1}{B(\frac{n-1}{2}, \frac{n-1}{2})} (s - s^2)^{\frac{n-3}{2}}, \quad (15)$$

which presents the same expectation and variation as the binary-based Binomial distribution when  $p = 0.5$  in Eq. (14), i.e., expectation of 0.5 and variation of  $1/4n$ .



(a) Probability mass function



(b) Cumulative distribution function

Fig. 8. Theoretical Binomial distributions for different  $n$ .

### B. Matching Score Normalization

Note that there exists an implicit assumption in the above analysis, i.e., all bits in the vector of length  $n$  are used for comparison, which is fine for global representations like DeepPrint [27] since there is no explicit meaning for each element. However, for the proposed localized representation, not all elements are considered during matching (see Eq. (3) and (6)). In some cases, overlapping area may be so small that few elements are used for comparison, which means the actual number of comparisons  $n'$  is limited, resulting in a very large variance  $p(1-p)/n'$ . Fig. 8 shows multiple theoretical Binomial distributions for different  $n$ .

Intuitively, matching between fingerprints with small overlapping area are uncertain and unreliable due to the limited number of feature elements being compared. It is a reasonable assumption that the size of overlapping area is directly proportional to the valid representation dimension in our localized representations. Fig. 9 presents the observed distributions of Hamming distance between impostor pairs on several typical datasets, including rolled (NIST SD4), plain (plain fingerprints in N2N Plain, i.e.,  $C_{2000}^2 = 1,999,000$  impostor pairs), and latent (NIST SD27). It can be observed that for pairs with different overlapping area sizes, the means of distributions are approximately equal to 0.5, while the variances vary significantly, which is consistent with Fig. 8.

Moreover, the Hamming distance in Fig. 9 is computed by subtracting the similarity from 1. This implies that its empirical cumulative probability is theoretically equivalent to

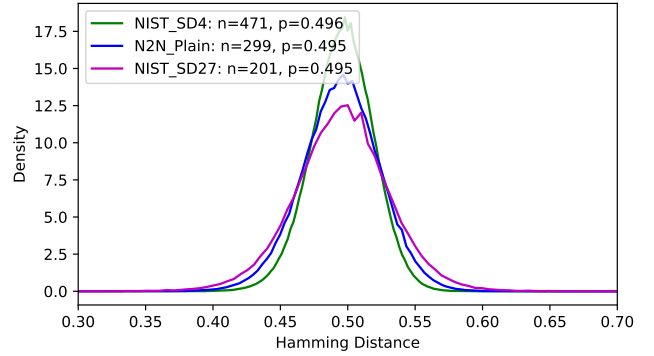


Fig. 9. Distributions of Hamming distance between impostor pairs.

FMR. However, varying FMRs are observed under the same Hamming distance for different  $n$ , i.e., the size of overlapping area in our method.

As previously discussed, the uncertainty of the matching score relies on the valid representation dimension, which is proportional to the size of the overlapping area. Thus, it is improper to use the matching score calculated with different overlapping areas, as seen in Eq. (7), which is also found in iris [42], [43]. These Binomial distributions differ only in their variances, making it a natural choice to normalize them. Therefore, we proposed to normalize the uncertainty of matching scores based on the size of overlapping area

$$\text{HD}_{\text{norm}} = 0.5 - (0.5 - \text{HD}_{\text{raw}}) \sqrt{\frac{s_o}{S_o}}, \quad (16)$$

where  $s_o$  denotes the size of overlapping area, and the normalization parameter  $S_o = 1326$  is the average of overlapping area over a large rolled fingerprint dataset (the total number of bits in the binarized LDRF is  $6 \times 16 \times 16 = 1536$ ).

Referring to Eq. (16), uncertainties in matching scores can be alleviated to achieve approximately equal FMRs under the same Hamming distance threshold. Matching scores between fingerprints with small overlapping area are normalized to be close to 0.5, whereas scores between fingerprints with larger overlapping area remain relatively unchanged. Similarly, for representations in real values, we also applied the same normalization as Eq. (16) since the variances also follow the similar form as Binomial distribution.

## V. EXPERIMENTAL RESULTS

In this section, we first introduce the datasets utilized in this paper, then the evaluation of matching performance on these datasets. We also show the results of ablation studies, qualitative analysis, and computational efficiency.

### A. Datasets

Multiple datasets with various impression types, including rolled, plain, latent, and contactless fingerprints, were utilized for evaluation. Table I shows the details of all datasets and fingerprint examples from these datasets are shown in Fig. 10.

We utilized the first 24,000 pairs rolled fingerprints in NIST SD14 for training. Fingerprint simulation described in

TABLE I  
FINGERPRINT DATASETS USED IN EXPERIMENTS.

Type	Dataset	Sensor	Description	Usage
Rolled	NIST SD4	Inking	2,000 pairs of rolled fingerprints	test
	NIST SD14	Inking	27,000 pairs of rolled fingerprints	train & test <sup>a</sup>
	N2N Rolled <sup>b</sup>	Optical	2,000 pairs of rolled fingerprints	test
Plain	FVC2000 <sup>c</sup>	Optical/Capacitive	100 fingers $\times$ 8 impressions	test
	FVC2002 <sup>c</sup>	Optical/Capacitive	100 fingers $\times$ 8 impressions	test
	FVC2004 <sup>c</sup>	Optical/Thermal sweeping	100 fingers $\times$ 8 impressions	test
	FVC2006 <sup>c</sup>	Electric field/Optical/Thermal sweeping	140 fingers $\times$ 12 impressions	test
	N2N Plain <sup>d</sup>	Optical	2,000 pairs (plain and rolled fingerprints)	test
	DPF <sup>†</sup>	Optical	776 rolled and 40,112 plain fingerprints with diverse poses	train & test <sup>e</sup>
Latent	NIST SD27 <sup>f</sup>	-	258 pairs (latent fingerprints from crime scene)	test
	N2N Latent <sup>g</sup>	-	2,000 rolled fingerprints and 3,383 latents from laboratory	test
	Hisign Latent <sup>†</sup>	-	10,458 pairs (latent fingerprints from crime scene)	test <sup>h</sup>
Contactless	PolyU CL2CB <sup>i</sup>	Optical/Camera	336 fingers $\times$ 6 contact-based and contactless fingerprints	test

<sup>a</sup> The first 24,000 pairs of rolled fingerprints for training, and the last 2,700 pairs for testing

<sup>b</sup> Subset U and V in NIST SD302b.

<sup>c</sup> DB1A, DB2A, and DB3A.

<sup>d</sup> Subset R and S in NIST SD302b.

<sup>e</sup> 32,676 plain fingerprints from randomly selected 633 fingers for training, and the rest 143 rolled fingerprints and 8 randomly selected plain fingerprints per finger for testing [41].

<sup>f</sup> 10,458 file fingerprints (plain or rolled) from Hisign latent dataset were added as background.

<sup>g</sup> Select 3,383 latent fingerprints from 10,000 latent fingerprints in NIST SD302e [36]

<sup>h</sup> The last 2,458 pairs for testing.

<sup>i</sup> Original contactless fingerprints are scaled to match the same mean ridge period of contact-based fingerprints [68], and no warping was performed.

<sup>†</sup> Corresponding datasets are private.

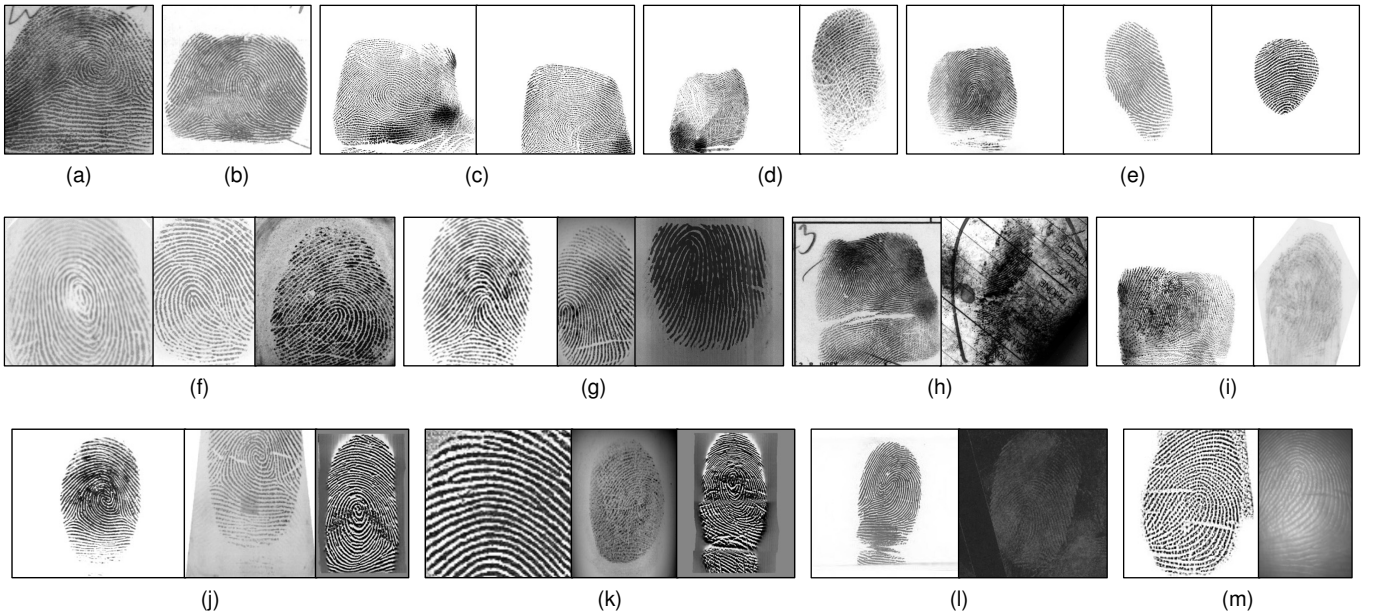


Fig. 10. Image examples from different fingerprint datasets (a) NIST SD4, (b) NIST SD14, (c) N2N Rolled, (d) N2N Plain, (e) DPF, (f) FVC2000, (g) FVC2002, (h) NIST SD27, (i) N2N Latent, (j) FVC2004, (k) FVC2006, (l) Hisign Latent, and (m) PolyU CL2CB.

Section III-E was applied to increase the diversity of training data. Note that no fine-tuning learning was applied on any other dataset. Considering that fingerprints in Diverse Poses Fingerprint dataset (DPF) [41] were collected with different 3D finger poses, i.e., diverse visible areas, therefore, we randomly selected 32,676 plain fingerprints from 633 fingers in DPF and employed their segmentation masks to simulate fingerprints with incomplete area (an example of the simulated partial fingerprint is shown in Fig. 3).

Apart from fingerprint datasets used in prior works, the

newly released fingerprint dataset N2N (NIST SD302) [69] consisting of rolled, plain, and latent fingerprints from 200 subjects with a total of 2,000 fingers, was also used for evaluation in this paper. Specifically, subset U was used as gallery, and subset V as rolled probe dataset (N2N Rolled). The combination of subset R and S contains 2,000 plain fingerprints and was used as plain probe dataset (N2N Plain).

Besides, there are a total of 10,000 latent fingerprints in NIST SD302e, but none of them is labeled with its corresponding finger identity. We followed the same selection strategy

proposed by Gu et al. [36], then 3,383 latent fingerprints were selected and labeled with their corresponding finger labels (N2N Latent). Additionally, we found that fingerprint orientations in N2N latent range from 0 to 360°, surpassing the defined orientation range based on prior knowledge (e.g.,  $\pm 60^\circ$  in [27]). Therefore, these latent fingerprints were first rotated by 0° and 180°, then the highest score was selected as the final result for all matching algorithms.

### B. Evaluation on Fingerprint Matching

Given the extracted fingerprint representations and valid area, fingerprint matching can be performed, including matching between fingerprints of same impression type (e.g., rolled to rolled) and different impression types (e.g., plain to rolled). Intuitively, compared to fingerprint matching between same type, matching between different types requires more accurate algorithms due to the large divergences on visible areas, ridge quality, and image acquisition.

Note that our matching score normalization method only achieves significant performance improvements when there are a numerous of impostor pairs that have limited overlapping area (i.e., at very low FMRs), while the sizes of datasets described in Section V-A are too small that such low FMRs cannot be measured using these limited impostor pairs. Therefore, the proposed matching score normalization was not evaluated on these datasets.

We followed the same experimental settings for FVC datasets in prior works [11], [60], i.e., the first impression of each finger was utilized for impostor matching. Specifically, for FVC2000, 2002, and 2004, the number of genuine pairs is  $100 \times C_8^2 = 2,800$ , and impostor pairs  $C_{100}^2 = 4,950$ . For FVC2006, the number of genuine pairs is  $140 \times C_{12}^2 = 9,240$ , and impostor pairs  $C_{140}^2 = 9,730$ . For PolyU CL2CB dataset [70], the number of genuine pairs is  $336 \times 6 \times 6 = 12,096$ , and impostor pairs  $336 \times 335 \times 6 \times 6 = 4,052,160$ .

Comparisons with previous fixed-length fingerprint representations were adopted, including DeepPrint [27], AFRNet [31], and multi-scale representation [36]. Considering that DeepPrint [27] and AFRNet [31] are not publicly available, we reimplemented them using the same training data to evaluate their performance on more datasets comprehensively. We do not utilize the feature realignment strategy proposed in [31] for fair comparison. The same fingerprint pose estimation [41] was utilized for Gu’s method [36] and the proposed method. Moreover, we adopt the fingerprint pose estimation method [41] instead of the original STN module for DeepPrint and AFRNet (denoted as V-DeepPrint and V-AFRNet) as well for further proof. The main reason for the performance difference between the values shown in the corresponding papers [27], [31] and ours is that the original DeepPrint and AFRNet were trained using a larger private dataset (more than 455,000 rolled fingerprints from 38,291 fingers for DeepPrint and 1,291,465 fingerprints of different types from 98,556 fingers for AFRNet), while only 48,000 rolled fingerprints from 24,000 fingers in NIST SD14 were utilized for training in this paper.

Furthermore, a minutia-based commercial matcher, VeriFinger SDK 12.0 [61], was also compared due to its SOTA

performance on prestigious evaluations [71], [72]. There are two types of matchers in VeriFinger SDK: ISO minutia-only template and proprietary template consisting of minutia and other features. In this paper, the proprietary template, which presents higher performance, was utilized for comparison.

We also tried to fuse the proposed method with the minutia-based matcher VeriFinger [61]. Considering that VeriFinger score cannot be utilized directly since it has been mapped to FMR and transformed by log function, i.e.,  $-12 \log(\text{FMR})$ , therefore, we learned a fusing function on N2N Rolled dataset

$$s = \text{Sigmoid}(-6.0f(s_1) - 7.5s_2 + 15.2), \quad (17)$$

where  $f(s_1) = 10^{s_1/100}$  is the remapped VeriFinger score  $s_1$ , and  $s_2$  denotes the matching score obtained by our method.

1) *Matching between Fingerprints of the Same Impression Type*: Table II and III show the matching performance between fingerprints of the same impression type. As shown in the tables, our method presents superior performance on all fingerprint datasets (except for FVC2000 DB1A, where the proposed method and Gu’s Multi-Scale method [36] present similar performance), and achieves comparable accuracy with the SOTA commercial minutia-based matcher, VeriFinger [61].

Compared with the reimplemented performance of DeepPrint [27] and AFRNet [31], superior performance can be observed using our method. Besides, extracting features from local regions was also considered by Gu et al. [36], however, non-fingerprint information will still be introduced in the extracted features due to the coarse division of local areas.

Intuitively, the proposed method alleviates the impact of background area during matching by removing the information outside overlapping area. The matching performance only drops slightly after template binarization thanks to the complete fingerprint area and high ridge quality. Moreover, the fusion of our method and VeriFinger [61] achieves higher or equal accuracy on all datasets, which indicates the proposed feature is complementary to the minutia-based representation.

2) *Matching between Fingerprints of Different Impression Types*: Table IV shows the matching performance between fingerprints of different impression types. Ridge enhancement and segmentation by FingerNet [23] was first applied on latent fingerprints to remove background noise, and followed by fingerprint matching based on both minutia-based and fixed-length representations.

As shown in the table, the proposed method also outperforms other fixed-length representation algorithms for fingerprints of different impression types. Since DeepPrint [27] and AFRNet [31] were trained on fingerprints with complete area, unsatisfactory performance was obtained for incomplete fingerprints such as non-frontal or latent fingerprints where the background area may dominate in the extracted features. For Gu’s multi-scale representation [36], in addition to the inappropriate local region division on fingerprints with small size (e.g., FVC2006 DB1A), its matching performance is also affected by the overlapping area threshold used in determining whether specific local regions are included in the final matching score. In some cases, improper thresholds may cause certain fingerprint features to be ignored or introduce

TABLE II  
VERIFICATION ACCURACY ON ROLLED FINGERPRINTS. TAR@FAR=0.01% IS REPORTED.

Method	Type	NIST SD4		NIST SD14		N2N Rolled <sup>1</sup>	
		TAR	Rank-1	TAR	Rank-1	TAR	Rank-1
VeriFinger [61]	Minutia-based	99.80	99.65	99.96	99.96	99.70	99.45
DeepPrint [27] <sup>2</sup>	Fixed-length	96.25	98.60	95.52	97.26	94.95	97.40
V-DeepPrint [27] <sup>3</sup>	Fixed-length	96.55	99.00	98.67	99.59	95.55	98.20
AFRNet [31] <sup>4</sup>	Fixed-length	94.75	97.40	97.00	97.78	96.25	96.85
V-AFRNet [31] <sup>5</sup>	Fixed-length	97.90	99.30	99.89	99.85	98.60	98.90
Multi-Scale [36]	Fixed-length	97.80	98.85	99.07	99.85	97.75	98.40
Ours (binary)	Fixed-length	99.35	99.40	99.85	99.85	98.55	98.50
Ours	Fixed-length	99.40	99.55	99.89	99.89	99.00	98.85
Fusion	-	99.80	99.75	99.96	100	-	-

<sup>1</sup> Used for learning the fusing function.

<sup>2</sup> Performance of DeepPrint reimplemented with STN using the same training data as our method to evaluate on more datasets.

<sup>3</sup> Performance of DeepPrint reimplemented without STN using the same data and the dense voting pose estimation results [41] as our method to evaluate on more datasets.

<sup>4</sup> Performance of AFRNet reimplemented without feature alignment using the same training data as our method to evaluate on more datasets.

<sup>5</sup> Performance of AFRNet reimplemented without feature alignment and STN using the same training data and the dense voting pose estimation results [41] as our method to evaluate on more datasets.

TABLE III  
VERIFICATION ACCURACY ON PLAIN FINGERPRINTS. TAR@FAR=0.1% IS REPORTED.

Method	Type	FVC2000			FVC2002			FVC2004			FVC2006		
		DB1A	DB2A	DB3A									
VeriFinger [61]	Minutia-based	99.89	99.96	99.50	99.89	99.93	99.43	98.93	97.79	99.86	92.65	100	99.47
DeepPrint [27]	Fixed-length	96.50	97.79	89.43	93.75	95.46	70.96	94.82	93.46	94.43	83.02	99.86	91.71
V-DeepPrint [27]	Fixed-length	96.03	96.67	90.10	94.71	97.67	69.85	94.00	91.10	96.32	82.39	99.76	90.21
AFRNet [31]	Fixed-length	99.18	98.82	97.14	98.04	99.46	80.25	98.14	96.04	96.46	93.31	99.99	94.57
V-AFRNet [31]	Fixed-length	88.36	96.18	84.64	76.82	90.54	49.82	87.43	79.25	92.32	59.49	99.27	89.81
Multi-Scale [36]	Fixed-length	99.00	99.68	91.57	98.89	99.61	83.36	97.36	94.75	94.46	47.37	99.92	92.48
Ours (binary)	Fixed-length	98.92	99.29	96.11	98.61	99.61	90.75	98.57	97.39	97.54	83.89	99.97	95.15
Ours	Fixed-length	98.79	99.46	97.29	99.18	99.68	94.93	98.64	98.29	97.50	88.92	100	96.09
Fusion	-	99.93	100	99.50	99.93	99.93	99.46	99.32	98.07	99.86	93.41	100	99.57

TABLE IV  
VERIFICATION ACCURACY ON FINGERPRINTS OF DIFFERENT IMPRESSION TYPES. TAR@FAR=0.1% IS REPORTED.

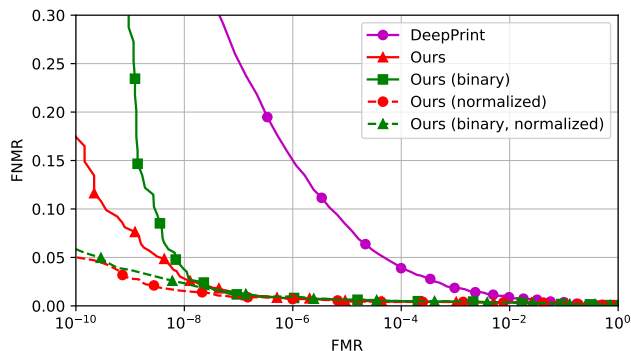
Method	Type	N2N Plain		DPF	PolyU	CL2CB	NIST SD27		N2N Latent		Hisign Latent	
		TAR <sup>1</sup>	Rank-1	TAR	TAR	Rank-1	TAR	Rank-1	TAR	Rank-1	TAR	Rank-1
VeriFinger [61]	Minutia-based	99.30	99.20	98.51	97.21	53.10	59.69	42.71	44.93	92.23	91.82	
DeepPrint [27]	Fixed-length	93.35	96.00	64.86	56.05	34.88	25.58	12.09	13.24	67.54	66.68	
V-DeepPrint [27]	Fixed-length	95.00	97.15	67.05	54.20	39.53	28.29	22.05	19.33	69.81	69.65	
AFRNet [31]	Fixed-length	96.90	97.40	77.36	52.61	45.35	35.66	13.04	15.37	74.00	72.25	
V-AFRNet [31]	Fixed-length	95.70	97.15	77.45	10.69	36.05	25.58	15.08	15.58	70.38	68.39	
Multi-Scale [36]	Fixed-length	97.80	98.10	87.68	64.13	44.57	43.80	17.20	26.54	78.76	83.81	
Ours (binary)	Fixed-length	97.47	97.95	88.72	77.15	36.43	36.05	21.84	26.23	83.32	79.94	
Ours	Fixed-length	98.15	98.20	91.52	87.71	53.88	42.64	29.17	27.82	89.75	87.43	
Ours (two branch)	Fixed-length	98.50	98.40	91.61	86.62	53.49	50.00	30.09	29.56	91.21	89.06	
Fusion	-	99.30	99.20	98.43	98.19	60.85	64.34	44.87	45.11	94.95	94.34	

<sup>1</sup> TAR@FAR=0.01%

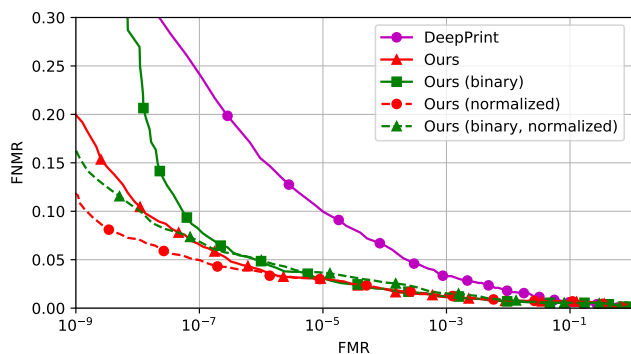
background information, ultimately reducing the matching performance.

In the cases of latent and contactless fingerprints, the matching performance of our method decreases after template binarization, due to the low ridge quality, background noise, and strong distortion. However, despite these challenges, the binarized LDRF still presents higher accuracy compared to prior works. It is also observed that fusing our method with

VeriFinger [61] improves the matching performance, which further demonstrates the complementarity of our deep localized feature and minutia information.



(a) NIST SD14 extended dataset



(b) N2N Plain extended dataset

Fig. 11. Fingerprint verification performance on extended datasets.

### C. Evaluation on Large-Scale Database

Fig. 11 shows the detection-error tradeoff (DET) curves of different algorithms on two extended datasets<sup>2</sup>. The proposed method and its three variations (matching based on real value and binary features, and normalized matching based on real value and binary features), are compared with DeepPrint [27]. Benefiting from the proposed normalization method, performance improvement is significant when FMR is small (from  $1 \times 10^{-7}$  to  $1 \times 10^{-10}$ ). For NIST SD14 extended dataset, FMR is reduced by almost two orders of magnitude at FNMR = 0.05 compared to matching before normalization, and reduced by five orders of magnitude compared to DeepPrint. While for N2N Plain extended dataset, FMR is reduced by an order of magnitude at FNMR = 0.1 compared to matching normalization, and four orders of magnitude compared to DeepPrint.

Fig. 12 shows several examples of impostor pairs, which present higher but unreliable matching scores due to the small overlapping area. Distributions of Hamming distance under different sizes of overlapping areas are also shown in Fig. 13. It can be observed that after matching score normalization, performance is improved since impostor scores with high uncertainty (small overlapping area) are penalized.

<sup>2</sup>VeriFinger [61] and Gu’s multi-scale [36] were not involved for comparison due to much matching time consumption

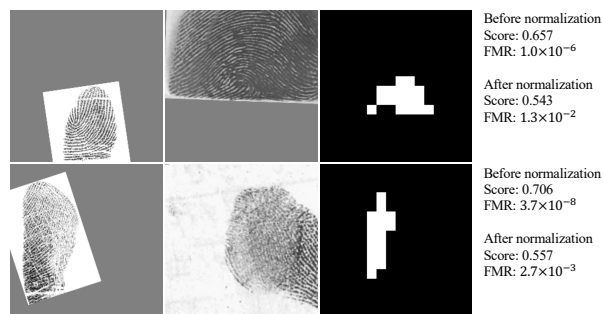
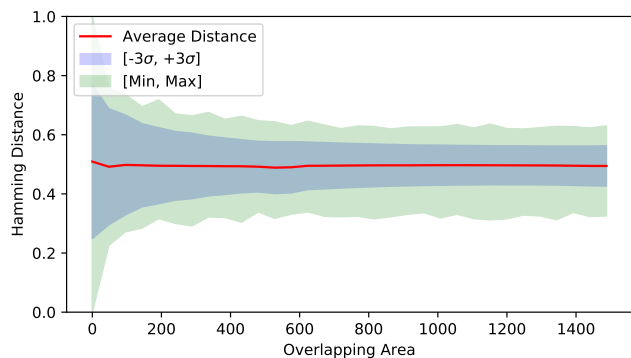
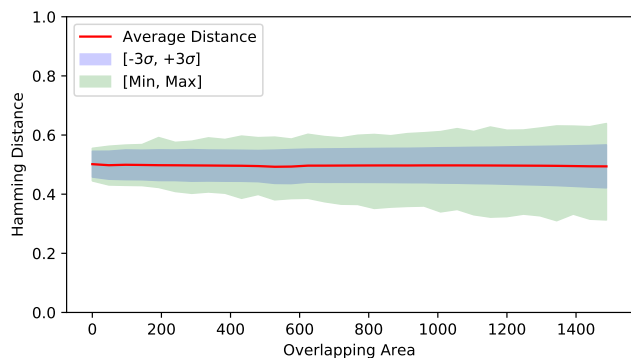


Fig. 12. Examples of impostor matching between fingerprints with higher but unreliable matching scores due to small overlapping area.



(a)



(b)

Fig. 13. Distributions of Hamming distance of impostor pairs under different sizes of overlapping areas (a) before and (b) after matching normalization.

### D. Ablation Study

We performed ablation studies to investigate the influence of several factors, including the dimension of representation, the number of fingers for training, the integration of 2D positional embedding, the effects of different combinations of losses, and the effects of fingerprint alignment accuracy. Performance of the proposed method was evaluated on five datasets, including NIST SD4, FVC2004 DB1A, DPF, Hisign Latent, and PolyU CL2CB.

1) *Representation Dimension*: Compared to global fixed-length representations like DeepPrint [27], our method has a higher feature dimension. Hence, we evaluated the matching performance with different representation dimensions. Table V shows the experimental results.

TABLE V  
VERIFICATION PERFORMANCE USING DIFFERENT DIMENSIONS OF REPRESENTATION.

Method	Dimension	NIST SD4	Hisign Latent	FVC2004 DB1A	DPF	PolyU CL2CB
		TAR@FAR=0.01%				
DeepPrint [27]	192	96.25	67.53	94.82	64.51	59.23
	512	93.45	65.83	94.46	63.46	58.89
Multi-Scale [36]	5120	97.80	78.76	97.36	87.68	64.13
Ours	512	99.20	86.21	97.00	90.03	83.32
	1024	99.35	89.22	98.69	90.82	82.81
	1792	99.40	89.75	98.64	91.52	87.71

TABLE VI  
ABLATION STUDY OF THE NUMBER OF TRAINING FINGERS AND SAMPLES PER FINGER.

Method	#Fingers	#Samples / Finger	NIST SD4	Hisign Latent	FVC2004 DB1A	DPF	PolyU CL2CB
			TAR@FAR=0.01%				
DeepPrint [27]	24,000	2	96.25	67.53	94.82	64.51	59.23
P-DeepPrint [27]	38,291	~12	98.70	-	97.50	-	-
Ours	3,600	2	97.90	75.31	91.75	87.67	47.02
	7,200	2	98.85	83.69	95.29	88.90	70.97
	14,400	2	99.10	87.96	98.00	90.47	73.46
	24,000	2	99.40	89.75	98.64	91.52	87.71

As shown in the table, our method presents higher performance with increasing representation dimensions. For fingerprints with good ridge quality, e.g., rolled and plain fingerprints, the reduction of matching performance using lower feature dimension is limited since sufficient and reliable information can be extracted. While for fingerprints with partial areas and poor ridge quality like latent fingerprints, significant performance reduction is observed with lower representation dimensions. Furthermore, it is observed that utilizing DeepPrint [27] with higher dimensions does not always result in performance improvement. The main reasons may be: (1) the number of trainable parameters in the final classification layer (FC layer) increases drastically, making it more difficult for training; (2) over-fitting may occur with higher feature dimensions, resulting in the extraction of outlier information and consequently reducing the matching performance.

2) *Number of Training Fingers*: More details can be retained in the extracted localized features compared to global fingerprint representations. We believe that it can increase the discriminating capability thus alleviating the requirement of training samples. Therefore, we also attempted to explore the effects of the number of training fingers. Table VI shows the results using different numbers of training fingers. As shown in the table, despite using only 1/3 of training fingers, the proposed localized representation can still present superior performance compared to DeepPrint [27], which was trained using all fingers in training set.

3) *2D Positional Embedding Module*: Global location information is incorporated in the last feature map through 2D positional embedding, which helps the network pay more attention to distinct details across different local regions. Table VII shows the performance results of not using the 2D positional embedding (PE) module and using the PE module at different positions. Significant performance improvements can be observed thanks to the proper incorporation of 2D

TABLE VII  
ABLATION STUDY RESULTS OF 2D POSITIONAL EMBEDDING.

PE	NIST SD4	Hisign Latent	FVC2004 DB1A	DPF	PolyU CL2CB
	TAR@FAR=0.1% (0.01% for NIST SD4)				
<sup>-1</sup>	99.20	85.27	95.14	88.20	81.22
<sup>I</sup> <sup>2</sup>	95.00	69.45	88.82	82.34	33.02
<sup>L</sup> <sup>3</sup>	99.40	89.75	98.64	91.52	87.71

<sup>1</sup> - means no PE module;

<sup>2</sup> <sup>I</sup> means setting the PE module at the beginning of the neural network to incorporate the location information in the first feature map;

<sup>3</sup> <sup>L</sup> means setting the PE module at the last of the neural network as Fig. 3 to incorporate the location information in the last feature map.

TABLE VIII  
ABLATION STUDY RESULTS OF LOSSES.

Losses		NIST SD4	Hisign Latent	FVC2004 DB1A	DPF	PolyU CL2CB
$\mathcal{L}_{\text{minu}}^*$	$\mathcal{L}_{\text{sim}}$	TAR@FAR=0.1% (0.01% for NIST SD4)				
$\times$	$\times$	98.25	73.27	89.04	79.11	24.77
$\checkmark$	$\times$	99.55	89.38	98.36	89.25	79.20
$\times$	$\checkmark$	99.55	89.06	98.43	89.69	64.62
$\checkmark$	$\checkmark$	99.40	89.75	98.64	91.52	87.71

\* If there is no  $\mathcal{L}_{\text{minu}}$ , there is no minutia branch as well.

positional embedding, especially for contactless and latent fingerprints. If the 2D PE module is set at the beginning of the neural network, the network may be more fragile to the slightly imprecise prediction of fingerprint pose, which severely degrades the performance of the network.

4) *The Effects of Different Combinations of Losses*: Classification loss and segmentation loss ( $\mathcal{L}_{\text{cls}}$  and  $\mathcal{L}_{\text{seg}}$ ) are basic for our method, so we study the other's effect on the matching performance. From Table VIII, it demonstrates the important

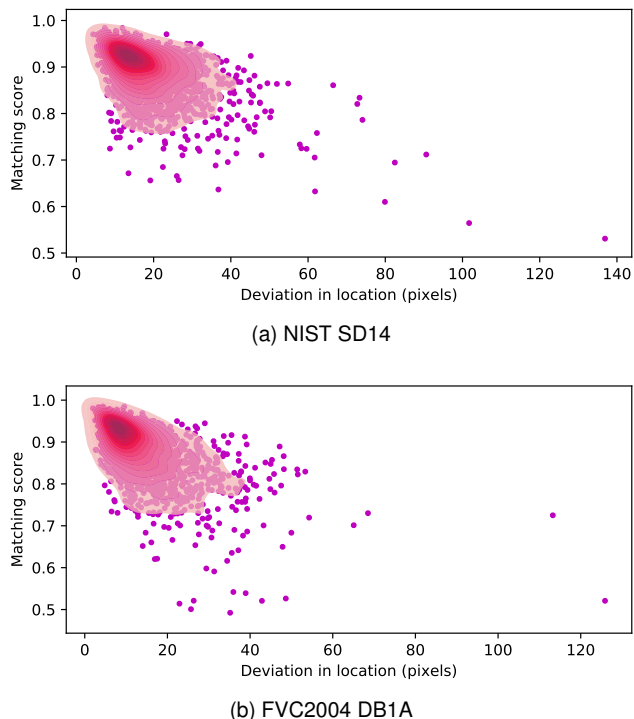


Fig. 14. Distribution of genuine scores under different alignment accuracies.

role of  $\mathcal{L}_{\text{minu}}$  which greatly improved the performance on each type of fingerprint dataset although the training data only includes the rolled one. Besides,  $\mathcal{L}_{\text{sim}}$  makes the network pay more attention to the similarity of each position on the localized dense descriptor which can further improve the matching accuracy.

5) *The Effects of Alignment Accuracy*: Then we explored the relationship between matching performance and fingerprint alignment accuracy. The average location deviation between matched minutia pairs, which are obtained by VeriFinger [61], was utilized to represent the fingerprint alignment accuracy of genuine pairs. Fig. 14 shows the distributions of genuine scores under different alignment accuracy. It is observed that genuine scores decrease with poor alignment, demonstrating the importance of fingerprint alignment in our method.

### E. Qualitative Analysis

Given the proposed probability modeling of distance between impostor pairs in Section IV, the recognition performance can be predicted solely based on genuine pairs. For example, Fig. 15 illustrates the DET curves of our method, depicting the predicted FMR range of  $[10^{-18}, 1]$ , on datasets containing limited number of impostor pairs. The reliable estimations of fingerprint matching performance at low FMR is essential for analyzing the evidential value of fingerprints, which is important for its application in forensic science [21].

Fig. 16 shows matching score distributions obtained by different representations. More concentrated and lower matching scores for impostor pairs can be observed using our method. The division margin between genuine and impostor scores is also enlarged thanks to the incorporation of fingerprint pose normalization and a better localized representation. For binary

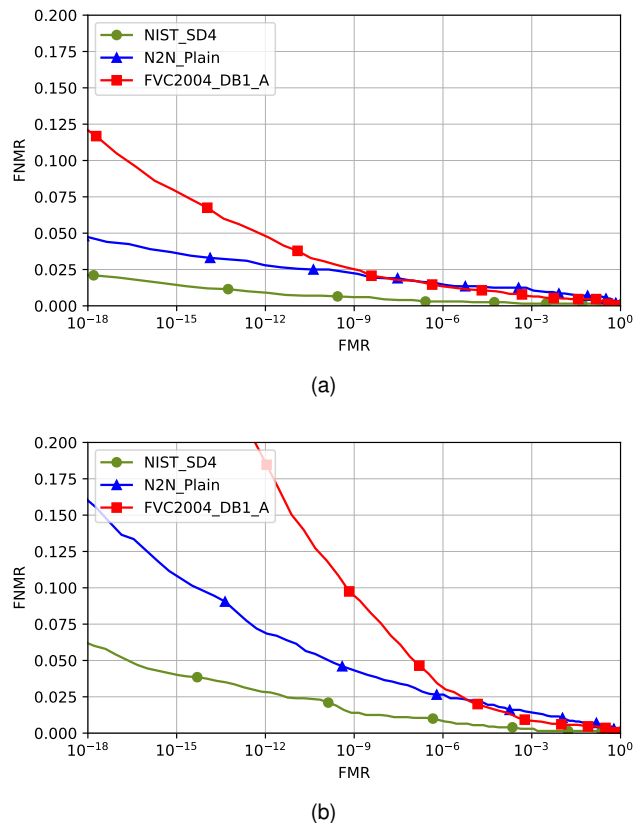


Fig. 15. Predicted DET curves using (a) real-value and (b) binary representations on different datasets with limited impostor pairs.

representations, it can be observed that genuine scores are reduced due to information loss, while impostor scores remains relatively unaffected. This phenomenon can be explained by the statistical analysis in Section IV.

For a better visualization, t-SNE was used to generate 2D low-dimensional representations of fingerprints obtained through various algorithms to evaluate their representation ability. Fig. 17 shows the 2D t-SNE visualizations of different fixed-length representations (800 impressions in FVC2004 DB1A) while maintaining the similarities calculated by different approaches. As depicted in the figure, our method significantly diminishes the likelihood of overlap between fingers by reducing the within-finger distance. And the available representation space was the most fully utilized by our method.

Fig. 18 shows several typical matching results using different representations. Note that comparing matching scores of different algorithms directly is not appropriate since they may have different similarity meanings. Therefore, FMR, which indicates the relative position of current genuine matching score in the overall impostor scores, is adopted for an intuitive performance comparison. As shown in the figure, the proposed method presents a lower FMR, which is consistent with the distribution of impostor scores in Fig. 16. And better performance can be observed using LDRF on fingerprints with diverse visible areas and limited overlapping area (e.g., DPF and latent fingerprints), whereas the global representation, DeepPrint [27], yields poor performance on such fingerprints. Besides, as previously mentioned, the small image size of

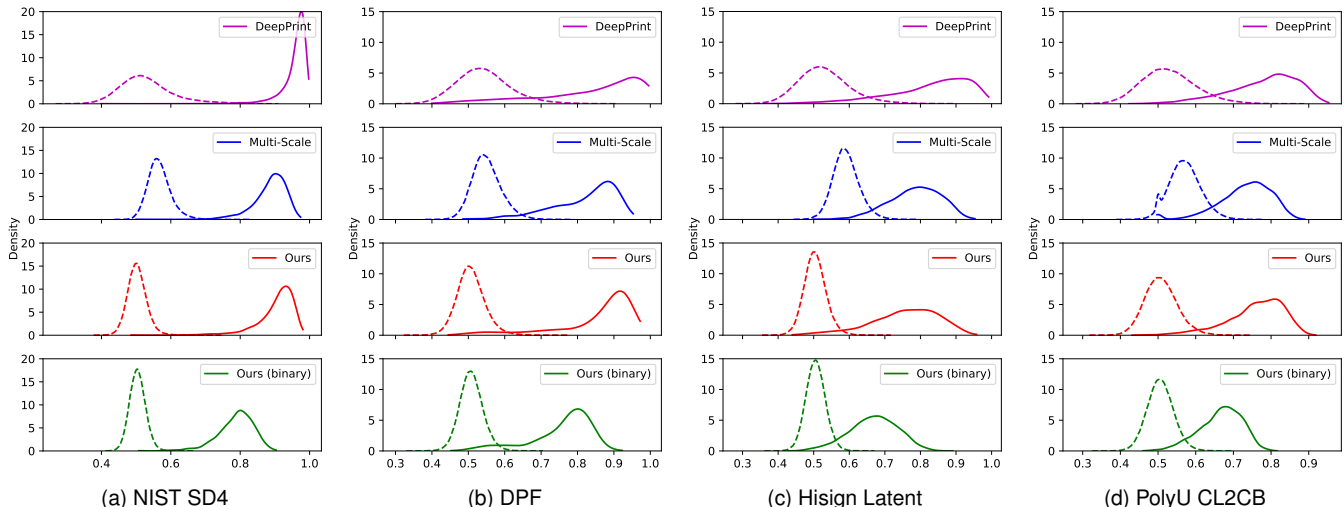


Fig. 16. Distributions of genuine matching scores (solid line) and impostor matching scores (dotted line) obtained using different fingerprint representations. VeriFinger [61] is not considered for comparison since its raw score has been mapped to FMR with mapping function unknown to us.

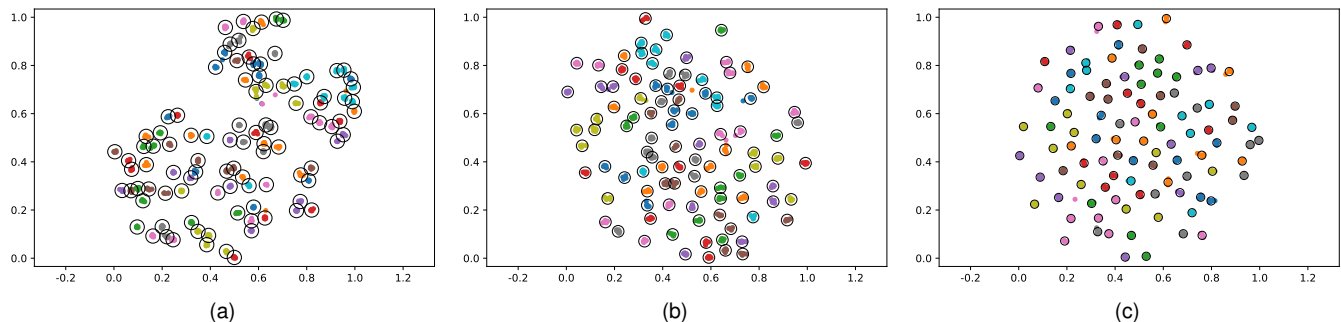


Fig. 17. 2D t-SNE visualization of 800 impressions from 100 fingers (FVC2004 DB1A) using (a) DeepPrint [27], (b) multi-scale [36], and (c) our method. Same color is used for impressions from the same finger. The black circle is used to highlight the threshold of TAR=98%.

fingerprints in FVC2006 DB1A, coupled with the limited overlapping area after alignment, hinders the effectiveness of coarse region division in multi-scale representation [36], which, in turn, reduces the matching performance instead of providing auxiliary assistance for fingerprint matching.

Fig. 19 shows several examples of the proposed localized deep representations. Consistent representations can be observed between genuine pairs, demonstrating the feasibility of determining similarity by comparing features at their respective locations.

#### F. Computational Efficiency

Table IX compares the computational efficiency of different algorithms, including DeepPrint [27], multi-scale [36], and our method on NIST SD14 dataset. All fingerprint representations were extracted using a 3.7GHz Intel Core i9-10900X CPU and NVIDIA GeForce 3090 GPU, and the matching process was conducted on the CPU. For multi-scale [36] and our method, the same fingerprint pose estimation algorithm [41] was utilized. Compared to minutia-based matching algorithms like VeriFinger [61], our method consumed significantly lower computational resources for matching descriptors, making it more appropriate for large-scale fingerprint identification

TABLE IX  
COMPUTATIONAL EFFICIENCY OF DIFFERENT APPROACHES (SECONDS).

Method	Pose Estimation	Representation Extraction	Descriptor Matching
VeriFinger [61]	-	1.13	$2.26 \times 10^{-4}$
DeepPrint [27]	-	$4.7 \times 10^{-2}$	$1.45 \times 10^{-7}$
Multi-Scale [36]	$3.2 \times 10^{-2}$	$5.7 \times 10^{-2}$	$3.44 \times 10^{-6}$
Ours	$3.2 \times 10^{-2}$	$1.1 \times 10^{-2}$	$1.16 \times 10^{-6}$
Ours (binary)	$3.2 \times 10^{-2}$	$1.1 \times 10^{-2}$	$1.27 \times 10^{-7}$

applications, where efficiency is crucial. The need for computational resources using our method can be reduced by the constrained matching within the overlapping area, while the binarized representation also significantly reduces the matching time consumption.

#### VI. LIMITATIONS AND FUTURE WORKS

Previous experimental results have demonstrated that our method achieve good performance on a variety of fingerprints with different visible areas and impression types. Nevertheless, there are still several problems to be tackled.

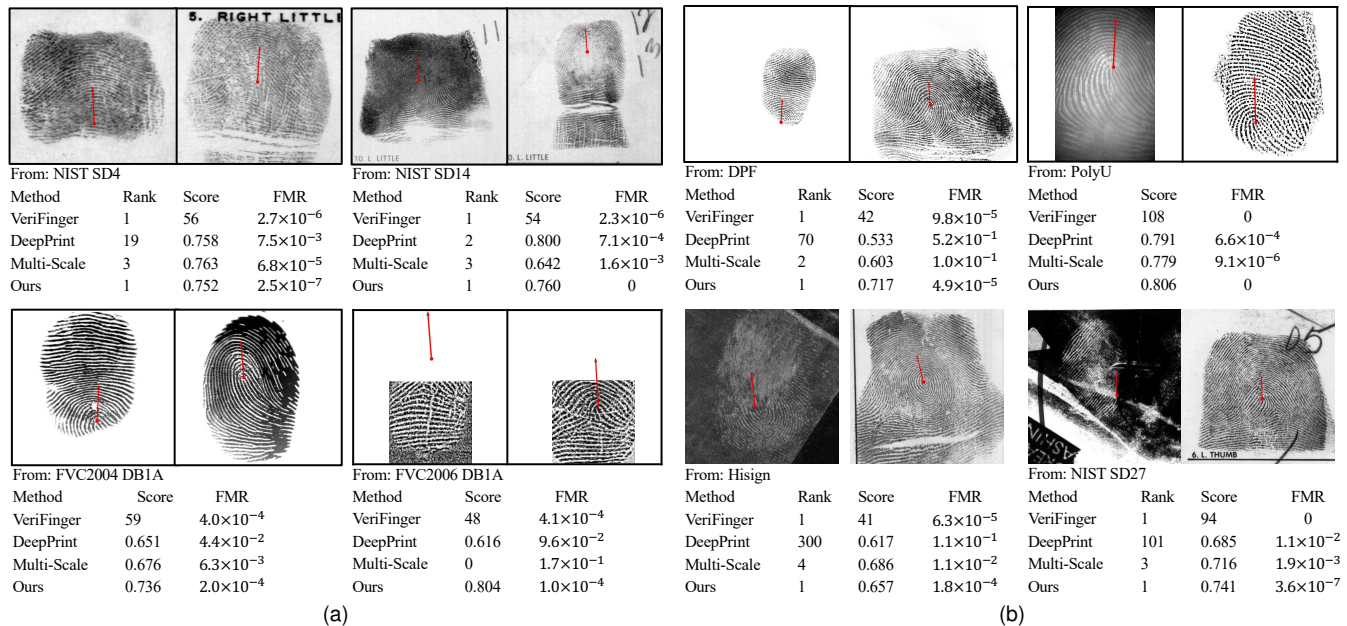


Fig. 18. Examples of matching results between fingerprints of (a) same and (b) different impression types.

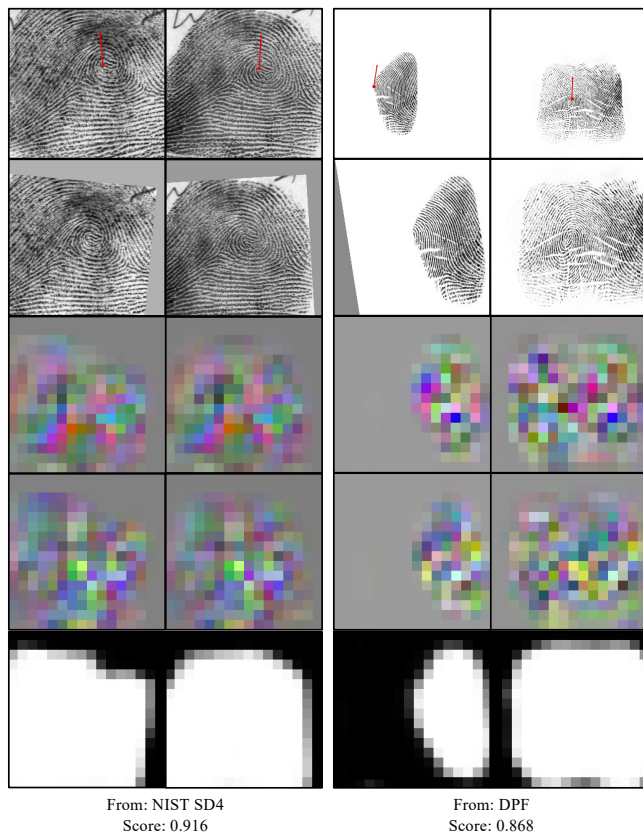


Fig. 19. Examples of the representations extracted from genuine pairs using our method. The first row shows the original fingerprint images with estimated fingerprint poses, and the second row shows the corresponding fingerprint alignment, and followed by the extracted dense representations and valid area.

Despite incorporating minutia information through the auxiliary minutia extraction task, the proposed LDRF still shows

potential for improving the matching performance in comparison to the commercial minutia-based matcher, VeriFinger [61]. Inaccurate fingerprint alignment, as discussed in Section V-D5, is possibly the main reason, due to the inaccurate estimation of fingerprint pose or strong skin distortion in this study. Several failure cases using our method are shown in Fig. 20.

However, matching algorithms based on minutia sets can be more flexible in dealing with problems of fingerprint alignment and skin distortion during matching. Therefore, rather than the naïve fusion proposed in Section V, a well-designed and in-depth integration between our localized deep representation and minutia-based representation will be explored in the future to further improve the matching accuracy.

Besides, extracting LDRF requires more computational resources compared to extracting minutiae, which can be performed on lightweight computing platforms. In the future, we also plan to reduce the complexity of our model to further improve its efficiency [73], [74].

Ridge enhancement was not performed on any of the experiments except on latent fingerprints. As traditional ridge enhancement algorithms were primarily designed for extracting minutiae accurately, therefore, it may be essential to explore a ridge enhancement technique that is more compatible with the proposed LDRF in the future.

## VII. CONCLUSION

Compared to minutiae-based fingerprint representations of variable length, fixed-length representations can efficiently match fingerprints in large-scale datasets. However, current fixed-length representations are affected by non-fingerprint areas when matching fingerprints of diverse visible areas and impression types. Therefore, we propose LDRF, a localized deep representation of the fingerprint extracted after fingerprint alignment. To introduce global constraints and help the

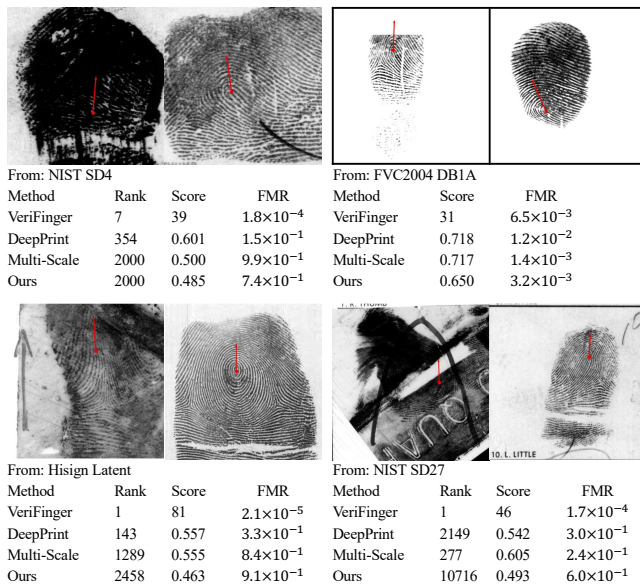


Fig. 20. Examples of failure cases with incorrect pose estimations, very small overlapping area, strong distortion, and complicated background noise.

network pay more attention to distinct characteristics across different local regions, a 2D positional embedding module was employed. The validity of the fingerprint area can aid in removing irrelevant and invalid information that is not useful or even harmful for fingerprint matching. Satisfactory matching performance can still be achieved after simple binarization to further enhance the efficiency of matching and feasibility of template encryption. Furthermore, by statistically modeling and analyzing matching scores using the proposed representations, we propose a matching score normalization technique that reduces uncertain matching scores between fingerprint pairs with different overlapping areas in large-scale datasets. Our fixed-length representation has been evaluated on 21 different datasets containing over 140K fingerprints of different impression types, including rolled, plain, latent, and contactless fingerprints. Experimental results show that LDRF outperforms other fixed-length representations and is robust to sensing technologies and impression types. The proposed normalization method reduces FMR significantly on large-scale fingerprint datasets consisting of over 5.11 million fingerprints, demonstrating its effectiveness and feasibility in improving identification performance for large population.

## REFERENCES

- [1] D. Maltoni, D. Maio, A. K. Jain, and J. Feng, *Handbook of Fingerprint Recognition*, 3rd ed. Springer Nature, Cham, Switzerland, 2022.
- [2] P. J. Grother, W. J. Salamon, C. I. Watson, M. D. Indovina, and P. A. Flanagan, "NIST IR 7477, Revision II, MINEX II Performance of Fingerprint Match-on-Card Algorithms-Phase IV Report," 2011.
- [3] S. Pankanti, S. Prabhakar, and A. K. Jain, "On the individuality of fingerprints," *IEEE Transactions on Pattern Analysis and Machine Intelligence*, vol. 24, no. 8, pp. 1010–1025, 2002.
- [4] L. Hong, Y. Wan, and A. Jain, "Fingerprint image enhancement: Algorithm and performance evaluation," *IEEE Transactions on Pattern Analysis and Machine Intelligence*, vol. 20, no. 8, pp. 777–789, 1998.
- [5] S. Chikkerur, A. N. Cartwright, and V. Govindaraju, "Fingerprint enhancement using STFT analysis," *Pattern Recognition*, vol. 40, no. 1, pp. 198–211, 2007.
- [6] N. K. Ratha, K. Karu, S. Chen, and A. K. Jain, "A real-time matching system for large fingerprint databases," *IEEE Transactions on Pattern Analysis and Machine Intelligence*, vol. 18, no. 8, pp. 799–813, 1996.
- [7] S.-H. Chang, F.-H. Cheng, W.-H. Hsu, and G.-Z. Wu, "Fast algorithm for point pattern matching: invariant to translations, rotations and scale changes," *Pattern Recognition*, vol. 30, no. 2, pp. 311–320, 1997.
- [8] ISO/IEC 19794-2:2011, "Information Technology—Biometric Data Interchange Formats—Part 2: Finger Minutiae Data," International Organization for Standardization, Standards.
- [9] S. A. Cole, "History of fingerprint pattern recognition," *Automatic Fingerprint Recognition Systems*, pp. 1–25, 2004.
- [10] Z. He, J. Zhang, L. Pang, and E. Liu, "PFVNet: A partial fingerprint verification network learned from large fingerprint matching," *IEEE Transactions on Information Forensics and Security*, vol. 17, pp. 3706–3719, 2022.
- [11] R. Cappelli, M. Ferrara, and D. Maltoni, "Fingerprint indexing based on minutia cylinder-code," *IEEE Transactions on Pattern Analysis and Machine Intelligence*, vol. 33, no. 5, pp. 1051–1057, 2010.
- [12] M. Liu and P.-T. Yap, "Invariant representation of orientation fields for fingerprint indexing," *Pattern Recognition*, vol. 45, no. 7, pp. 2532–2542, 2012.
- [13] J. Feng, "Combining minutiae descriptors for fingerprint matching," *Pattern Recognition*, vol. 41, no. 1, pp. 342–352, 2008.
- [14] K. Cao and A. K. Jain, "Automated latent fingerprint recognition," *IEEE Transactions on Pattern Analysis and Machine Intelligence*, vol. 41, no. 4, pp. 788–800, 2019.
- [15] S. Rane, Y. Wang, S. C. Draper, and P. Ishwar, "Secure biometrics: Concepts, authentication architectures, and challenges," *IEEE Signal Processing Magazine*, vol. 30, no. 5, pp. 51–64, 2013.
- [16] K. Nandakumar, A. K. Jain, and S. Pankanti, "Fingerprint-based fuzzy vault: Implementation and performance," *IEEE Transactions on Information Forensics and Security*, vol. 2, no. 4, pp. 744–757, 2007.
- [17] S. Pankanti, S. Prabhakar, and A. Jain, "On the individuality of fingerprints," *IEEE Transactions on Pattern Analysis and Machine Intelligence*, vol. 24, no. 8, pp. 1010–1025, 2002.
- [18] S. Dass, Y. Zhu, and A. Jain, "Statistical models for assessing the individuality of fingerprints," in *Fourth IEEE Workshop on Automatic Identification Advanced Technologies (AutoID'05)*, 2005, pp. 3–9.
- [19] S. C. Dass, "Assessing fingerprint individuality in presence of noisy minutiae," *IEEE Transactions on Information Forensics and Security*, vol. 5, no. 1, pp. 62–70, 2010.
- [20] National Research Council, *Strengthening forensic science in the United States: A path forward*. National Academies Press, 2009.
- [21] A. Nagar, H. Choi, and A. K. Jain, "Evidential value of automated latent fingerprint comparison: An empirical approach," *IEEE Transactions on Information Forensics and Security*, vol. 7, no. 6, pp. 1752–1765, 2012.
- [22] A. Sankaran, P. Pandey, M. Vatsa, and R. Singh, "On latent fingerprint minutiae extraction using stacked denoising sparse autoencoders," in *2014 IEEE International Joint Conference on Biometrics (IJCB)*. IEEE, 2014, pp. 1–7.
- [23] Y. Tang, F. Gao, J. Feng, and Y. Liu, "Fingernet: An unified deep network for fingerprint minutiae extraction," in *2017 IEEE International Joint Conference on Biometrics (IJCB)*. IEEE, 2017, pp. 108–116.
- [24] K. Cao and A. K. Jain, "Fingerprint indexing and matching: An integrated approach," in *2017 IEEE International Joint Conference on Biometrics (IJCB)*. IEEE, 2017, pp. 437–445.
- [25] R. Cappelli, "Fast and accurate fingerprint indexing based on ridge orientation and frequency," *IEEE Transactions on Systems, Man, and Cybernetics, Part B (Cybernetics)*, vol. 41, no. 6, pp. 1511–1521, 2011.
- [26] D. Song and J. Feng, "Fingerprint indexing based on pyramid deep convolutional feature," in *2017 IEEE International Joint Conference on Biometrics (IJCB)*. IEEE, 2017, pp. 200–207.
- [27] J. J. Engelsma, K. Cao, and A. K. Jain, "Learning a fixed-length fingerprint representation," *IEEE Transactions on Pattern Analysis and Machine Intelligence*, vol. 43, no. 6, pp. 1981–1997, 2021.
- [28] D. Song, Y. Tang, and J. Feng, "Aggregating minutia-centred deep convolutional features for fingerprint indexing," *Pattern Recognition*, vol. 88, pp. 397–408, 2019.
- [29] R. Li, D. Song, Y. Liu, and J. Feng, "Learning global fingerprint features by training a fully convolutional network with local patches," in *2019 International Conference on Biometrics (ICB)*. IEEE, 2019, pp. 1–8.
- [30] S. Wu, B. Liu, Z. Wang, Z. Jia, and J. Feng, "Minutiae-awarely learning fingerprint representation for fingerprint indexing," in *2022 IEEE International Joint Conference on Biometrics (IJCB)*. IEEE, 2022, pp. 1–8.

- [31] S. A. Grosz and A. K. Jain, "Afr-net: Attention-driven fingerprint recognition network," *IEEE Transactions on Biometrics, Behavior, and Identity Science*, pp. 1–1, 2023.
- [32] Y. Sutcu, S. Rane, J. S. Yedidia, S. C. Draper, and A. Vetro, "Feature extraction for a Slepian-Wolf biometric system using LDPC codes," in *2008 IEEE International Symposium on Information Theory*. IEEE, 2008, pp. 2297–2301.
- [33] Z. Jin, A. B. J. Teoh, T. S. Ong, and C. Tee, "A revocable fingerprint template for security and privacy preserving," *KSH Transactions on Internet and Information Systems (TIIS)*, vol. 4, no. 6, pp. 1327–1342, 2010.
- [34] Y. Imamverdiyev, A. B. J. Teoh, and J. Kim, "Biometric cryptosystem based on discretized fingerprint texture descriptors," *Expert Systems with Applications*, vol. 40, no. 5, pp. 1888–1901, 2013.
- [35] A. K. Jain, S. Prabhakar, L. Hong, and S. Pankanti, "FingerCode: A filterbank for fingerprint representation and matching," in *Proceedings of the IEEE Computer Society Conference on Computer Vision and Pattern Recognition*, vol. 2. IEEE, 1999, pp. 187–193.
- [36] S. Gu, J. Feng, J. Lu, and J. Zhou, "Latent fingerprint indexing: Robust representation and adaptive candidate list," *IEEE Transactions on Information Forensics and Security*, vol. 17, pp. 908–923, 2022.
- [37] Y. Wang, J. Hu, and D. Phillips, "A fingerprint orientation model based on 2D Fourier expansion (FOMFE) and its application to singular-point detection and fingerprint indexing," *IEEE Transactions on Pattern Analysis and Machine Intelligence*, vol. 29, no. 4, pp. 573–585, 2007.
- [38] A. Kumar and Y. Zhou, "Contactless fingerprint identification using level zero features," in *CVPR 2011 WORKSHOPS*, 2011, pp. 114–119.
- [39] J. Bringer and V. Despiegel, "Binary feature vector fingerprint representation from minutiae vicinities," in *2010 Fourth IEEE International Conference on Biometrics: Theory, Applications and Systems (BTAS)*. IEEE, 2010, pp. 1–6.
- [40] F. Farooq, R. M. Bolle, T.-Y. Jea, and N. Ratha, "Anonymous and revocable fingerprint recognition," in *2007 IEEE Conference on Computer Vision and Pattern Recognition*. IEEE, 2007, pp. 1–7.
- [41] Y. Duan, J. Feng, J. Lu, and J. Zhou, "Estimating fingerprint pose via dense voting," *IEEE Transactions on Information Forensics and Security*, vol. 18, pp. 2493–2507, 2023.
- [42] J. Daugman, "New methods in iris recognition," *IEEE Transactions on Systems, Man, and Cybernetics, Part B (Cybernetics)*, vol. 37, no. 5, pp. 1167–1175, 2007.
- [43] —, "How iris recognition works," in *The Essential Guide to Image Processing*. Elsevier, 2009, pp. 715–739.
- [44] S. A. Grosz, J. J. Engelsma, R. Ranjan, N. Ramakrishnan, M. Aggarwal, G. G. Medioni, and A. K. Jain, "Minutiae-guided fingerprint embeddings via vision transformers," *arXiv preprint arXiv:2210.13994*, 2022.
- [45] A. Dosovitskiy, L. Beyer, A. Kolesnikov, D. Weissenborn, X. Zhai, T. Unterthiner, M. Dehghani, M. Minderer, G. Heigold, S. Gelly *et al.*, "An image is worth 16x16 words: Transformers for image recognition at scale," in *International Conference on Learning Representations*, 2020.
- [46] X. Yang, J. Feng, and J. Zhou, "Localized dictionaries based orientation field estimation for latent fingerprints," *IEEE Transactions on Pattern Analysis and Machine Intelligence*, vol. 36, no. 5, pp. 955–969, 2014.
- [47] Q. Yin, J. Feng, J. Lu, and J. Zhou, "Orientation field estimation for latent fingerprints by exhaustive search of large database," in *Proceedings of the IEEE International Conference on Biometrics Theory, Applications and Systems (BTAS)*, 2018, pp. 1–9.
- [48] Y. Duan, J. Feng, J. Lu, and J. Zhou, "Orientation field estimation for latent fingerprints with prior knowledge of fingerprint pattern," in *2021 IEEE International Joint Conference on Biometrics (IJCB)*. IEEE, 2021, pp. 1–8.
- [49] X. Si, J. Feng, J. Zhou, and Y. Luo, "Detection and rectification of distorted fingerprints," *IEEE Transactions on Pattern Analysis and Machine Intelligence*, vol. 37, no. 3, pp. 555–568, 2015.
- [50] X. Si, J. Feng, B. Yuan, and J. Zhou, "Dense registration of fingerprints," *Pattern Recognition*, vol. 63, pp. 87–101, 2017.
- [51] S. Gu, J. Feng, J. Lu, and J. Zhou, "Efficient rectification of distorted fingerprints," *IEEE Transactions on Information Forensics and Security*, vol. 13, no. 1, pp. 156–169, 2017.
- [52] X. Guan, Y. Duan, J. Feng, and J. Zhou, "Direct regression of distortion field from a single fingerprint image," in *2022 IEEE International Joint Conference on Biometrics (IJCB)*. IEEE, 2022, pp. 1–8.
- [53] Q. Yin, J. Feng, J. Lu, and J. Zhou, "Joint estimation of pose and singular points of fingerprints," *IEEE Transactions on Information Forensics and Security*, vol. 16, pp. 1467–1479, 2021.
- [54] K. He, X. Zhang, S. Ren, and J. Sun, "Deep residual learning for image recognition," in *Proceedings of the IEEE Conference on Computer Vision and Pattern Recognition*, 2016, pp. 770–778.
- [55] A. Vaswani, N. Shazeer, N. Parmar, J. Uszkoreit, L. Jones, A. N. Gomez, Ł. Kaiser, and I. Polosukhin, "Attention is all you need," *Advances in Neural Information Processing Systems*, vol. 30, 2017.
- [56] Z. Wang and J.-C. Liu, "Translating math formula images to latex sequences using deep neural networks with sequence-level training," *International Journal on Document Analysis and Recognition (IJ DAR)*, vol. 24, no. 1-2, pp. 63–75, 2021.
- [57] A. Munoz-Briseno, A. Gago-Alonso, and J. Hernández-Palancar, "Fingerprint indexing with bad quality areas," *Expert Systems with Applications*, vol. 40, no. 5, pp. 1839–1846, 2013.
- [58] O. Iloanusi, A. Gyaourova, and A. Ross, "Indexing fingerprints using minutiae quadruplets," in *CVPR 2011 WORKSHOPS*. IEEE, 2011, pp. 127–133.
- [59] R. Cappelli, M. Ferrara, and D. Maltoni, "Minutia Cylinder-Code: A new representation and matching technique for fingerprint recognition," *IEEE Transactions on Pattern Analysis and Machine Intelligence*, vol. 32, no. 12, pp. 2128–2141, 2010.
- [60] Y. Su, J. Feng, and J. Zhou, "Fingerprint indexing with pose constraint," *Pattern Recognition*, vol. 54, pp. 1–13, 2016.
- [61] VeriFinger SDK 12.0, <https://www.neurotechnology.com/verifinger.html>.
- [62] O. Ronneberger, P. Fischer, and T. Brox, "U-Net: Convolutional networks for biomedical image segmentation," in *International Conference on Medical Image Computing and Computer-Assisted Intervention (MICCAI)*. Springer, 2015, pp. 234–241.
- [63] J. Daugman, "Collision avoidance on national and global scales: Understanding and using big biometric entropy," *TechRxiv preprint TechRxiv:14061671.v1*, 2021.
- [64] Y. Wen, K. Zhang, Z. Li, and Y. Qiao, "A discriminative feature learning approach for deep face recognition," in *Computer Vision—ECCV 2016*. Springer, 2016, pp. 499–515.
- [65] W. Liu, Y. Wen, Z. Yu, M. Li, B. Raj, and L. Song, "Sphereface: Deep hypersphere embedding for face recognition," in *Proceedings of the IEEE Conference on Computer Vision and Pattern Recognition*, 2017, pp. 212–220.
- [66] H. Wang, Y. Wang, Z. Zhou, X. Ji, D. Gong, J. Zhou, Z. Li, and W. Liu, "Cosface: Large margin cosine loss for deep face recognition," in *Proceedings of the IEEE Conference on Computer Vision and Pattern Recognition*, 2018, pp. 5265–5274.
- [67] M. C. Spruill, "Asymptotic distribution of coordinates on high dimensional spheres," *Electronic Communications in Probability*, vol. 12, pp. 234–247, 2007.
- [68] Z. Cui, J. Feng, and J. Zhou, "Monocular 3D fingerprint reconstruction and unwarping," *IEEE Transactions on Pattern Analysis and Machine Intelligence*, 2023.
- [69] G. Fiumara, P. Flanagan, J. Grantham, K. Ko, K. Marshall, M. Schwarz, E. Tabassi, B. Woodgate, and C. Boehnen, "National Institute of Standards and Technology Special Database 302: Nail to Nail Fingerprint Challenge: 2007," Tech. Rep., 2018.
- [70] C. Lin and A. Kumar, "Matching contactless and contact-based conventional fingerprint images for biometrics identification," *IEEE Transactions on Image Processing*, vol. 27, no. 4, pp. 2008–2021, 2018.
- [71] B. Dorizzi, R. Cappelli, M. Ferrara, D. Maio, D. Maltoni, N. Houmani, S. Garcia-Salicetti, and A. Mayoue, "Fingerprint and on-line signature verification competitions at ICB 2009," in *Proceedings of the Third International Conference on Biometrics (ICB)*, 2009, pp. 725–732.
- [72] C. Watson, G. Fiumara, E. Tabassi, S. Cheng, P. Flanagan, and W. Salamon, "Fingerprint vendor technology evaluation, NIST interagency/internal report 8034: 2015," 2014.
- [73] S. Han, H. Mao, and W. J. Dally, "Deep compression: Compressing deep neural networks with pruning, trained quantization and Huffman coding," *International Conference on Learning Representations (ICLR)*, 2016.
- [74] A. G. Howard, M. Zhu, B. Chen, D. Kalenichenko, W. Wang, T. Weyand, M. Andreetto, and H. Adam, "Mobilenets: Efficient convolutional neural networks for mobile vision applications," *arXiv preprint arXiv:1704.04861*, 2017.